MUMFORD-SHAH MODEL AND ITS APPLICATION IN IMAGE PROCESSING

Qinghui Zhang

A thesis
in
The Department
of
Computer Science and software Engineering

Presented in Partial Fulfillment of the Requirements
For the Degree of Master of Computer Science
Concordia University
Montréal, Québec, Canada

May 2005

Your file Votre référence
ISBN: 0-494-10301-9
Our file Notre référence
ISBN: 0-494-10301-9

Abstract

Mumford-Shah Model and its Application in Image Processing

Qinghui Zhang

The Mumford-Shah (MS) model has been studied in details in this thesis. It is found that the piecewise constant approximation MS model can not be used for images with large variation in the intensities. Therefore a linear approximation MS model is introduced. We have found that the linear approximation MS model provides better segmentation results than the piecewise constant MS model. The level set methods are used in the numerical computations. We have explicitly proved that the MS energy decreases with time (iterations) for all cases. The μ and ν dependence of the MS model is also studied. It is found that when μ becomes large, the piecewise constant model is recovered. On the other hand, if μ tends to zero, detailed structure of the input image can be obtained by the MS segmentation model. The MS and the Rudin-Osher-Fatemi (ROF) like models are generalized to include high order derivative terms. It is found that this kind of model can be used for edges with low contrast. The MS model is also generalized to a new model which can be used to detect roof edges which are difficult to detect by other models. Verification of the proposed models is done based on experimental results.

Acknowledgments

I would like to express my sincere gratitude to my advisor Professor Tien D. Bui for his guidance, help and support.

I thank my fellow student Song Gao for many wonderful collaborations and discussions. I would also like to thank XiaoJun Du, Dongwook Cho, WuMo Pan of the Professor Bui's group for useful discussions. I also like to thank Shuo Li and Chao Jin for the pleasure talks that we had in the lab.

I thank my wife and my daughter for their supports and encouragements.

Contents

List of Figures

Chapter 1

Introduction

In this chapter we will briefly review the basic concepts of image segmentation and the level set method and outline the purpose of this thesis.

1.1 Image Segmentation

Image processing is one of the most important branches in computer science application fields [42]. One of the difficult problems of image processing is image segmentation [41]. Although image segmentation has been studied for many years, it still lacks fundamental theoretical background. This does not prevent it from being widely used in many fields such as medical image processing, computer vision etc. Actually it is very difficult to give a formal definition of segmentation.

In general, we think that image segmentation is to find the boundary of objects that are of interest. But different people may have interest in different things. Thus the segmentation problem is an observer dependent problem. This makes the image segmentation problem more difficult. More or less, we believe that the following "definition" reflects what most people want. That is we want to divide a given image into several regions. In those regions, the image can be approximated by smooth functions. The process of finding the boundaries of those regions is called image segmentation.

To solve this problem, many models have been suggested such as snakes [10, 20], the geodesic active contours model [2, 3, 4, 5], the Mumford-Shah models [13] etc. All those models construct some kind of energy functionals and try to minimize them. It

is well known that all those models are ill-posed. In other words, there are many local minima of the energy functionals. However, despite this shortcoming, those methods are still used in image segmentation.

In this thesis, we will study the Mumford-Shah model which was put forward in 1989 [13] and now is widely used in computer vision and image segmentation. In this model, we will try to find the minimum Mumford-Shah energy for each input image. It is well known that minimization of an energy function will lead to an Euler-Lagrange partial differential equation (PDE). We will use the level set technique in solving the related PDE's.

1.2 The Level Set Methods

The level set methods are the numerical techniques originally introduced by Osher and Sethian [14, 32, 33, 34, 35, 47] for analyzing and computing the motion of interfaces. The basic idea of the Level set methods is the following: Define a level set function $\phi(x, y, t)$ in a input image (say 2-dimension) as

$$\phi(x,y,t) \quad \left\{ \begin{array}{l} > 0 \text{ if } (x,y) \text{ in } \Omega \\ = 0 \text{ if } (x,y) \text{ in } \delta\Omega \\ < 0 \text{ if } (x,y) \text{ in } \bar{\Omega} \end{array} \right\}, \tag{1}$$

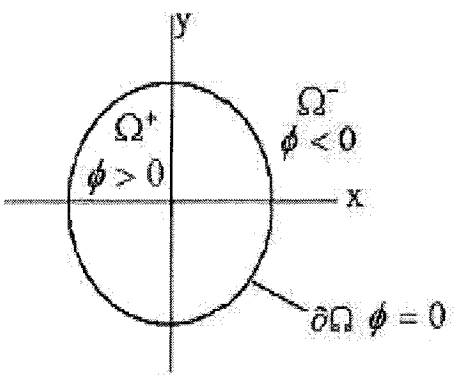

Figure 1: *The level set function* $\phi(x, y, t)$.

Then the evolution of the level set function can be used to determine the movement

of the front. Since the function $\phi(x, y, t)$ at the boundary of the object must be zero, thus we have the following equation:

$$\frac{\partial \phi(x, y, t)}{\partial t} + \nabla \phi \cdot (\frac{dx}{dt}, \frac{dy}{dt}) = 0 \tag{2}$$

Eq.(2) can be re-written as

$$\frac{\partial \phi(x, y, t)}{\partial t} + F|\nabla \phi| = 0, \tag{3}$$

where, $F = \vec{n} \cdot \vec{v}$ ($\vec{v} = (\frac{dx}{dt}, \frac{dy}{dt})$ is the velocity of the boundary, $\vec{n}$ is the unit normal to the boundary) is the normal velocity of the boundary. To solve Eq.(3), we still need the initial condition $\phi(x, y, 0) = \phi_0(x, y)$ and boundary condition such as $\frac{\partial \Phi}{\partial \vec{n}} = 0$ on $\delta\Omega$.

The advantages of the level set methods on propagating boundaries are the following: (1) the topological changes in the evolving boundary such as merging and breaking are handled naturally; (2) It is easy to build accurate numerical schemes to approximate the equations of motion. Here we need to point out that F is determined by the dynamics of the system which is assumed to be known in advance.

1.3 Purpose of the Thesis

In this thesis, we will study the Mumford-Shah model systematically. We have derived in detail all the necessary mathematical tools for the image segmentation problem. Detail experimental analyses of the Mumford-Shah model are also given. We have also tried to generalize the Mumford-Shah model to be able to detect edges of images with low contrast. Our experimental results support the validation of these generalizations.

This thesis is arranged in the following way: In the Chapter II, a short introduction to the Mumford-Shah model is given and the piecewise constant approximation of the Mumford-Shah model is studied. In Chapter III, the piecewise linear approximation of the Mumford-Shah model is developed and tested. The dependencies of the Mumford-Shah model on the parameters μ and ν are studied in Chapter IV. Some constraints on the parameters μ and ν are also given in this chapter. In Chapter V, some variations and generalizations of the Mumford-Shah model are developed. Conclusions and possible future development are discussed in the last chapter.

Chapter 2

The Mumford-Shah Model and the Constant Approximation

2.1 Introduction

The segmentation problem is a very important topic in many different areas including computer vision, medical imaging, video processing etc. This problem can be defined in the following way: For an observed image u_0 (possibly with noise), we want to find an optimal piecewise smooth approximation u of u_0 for each specific region. The regions are denoted by $\Omega_i, i = 1, 2, ..., n$. The function u varies smoothly within each Ω_i and rapidly or discontinuously across the boundaries of Ω_i. The process of finding the boundaries of Ω_i is called segmentation. The boundaries of all Ω_i are denoted by C and Ω_i is an open set. Therefore the whole image can be expressed as

$$\Omega = \bigcup \Omega_i \bigcup C. \tag{4}$$

To solve this problem Mumford and Shah have proposed the following minimization problem [13]:

$$\begin{aligned} inf_{u,C}\{E(u,C) &= \alpha \int_{\Omega \setminus C} (u - u_0)^2 dxdy + \mu \int_{\Omega \setminus C} |\nabla u|^2 dxdy + \nu |C|\}, \\ &= \alpha \sum_i \int_{\Omega_i} (u - u_0)^2 dxdy + \mu \sum_i \int_{\Omega_i \setminus C} |\nabla u|^2 dxdy + \nu |C|\}, \end{aligned} \tag{5}$$

where $\mu, \nu, \alpha > 0$ are fixed parameters which can be described as weight factors. The problem is to find u and C such that the above energy is minimal. C is the segmentation curve and u is the approximation of u_0.

From Eq.(5), we have the following observations. To minimize $E(u, C)$, we need: (1) u is a good approximation of u_0, (2) u does not vary much in each region Ω_i, and (3) the boundary of each region Ω_i should be as short as possible. The minimal value of $E(u, C)$ should depend on the values of α, μ and ν.

2.2 Markov Random Field model

The Mumford-Shah model can be understood in the following way: For an observed image u_0 (could be noisy), we want to find the approximate image u (or segmentation image u). Using Bayesian decision theorem, the posterior probability is

$$P(u|u_0) = P(u_0|u)P(u). \tag{6}$$

Here $P(u)$ is the probability of obtaining u for different u_0, and $P(u_0|u)$ is the probability of obtaining u_0 with the segmentation image u. Then $P(u|u_0)$ is the probability of obtaining the image u with input image u_0. If we assume that $P(u)$ is proportional to its energy in the following form

$$P(u) = \exp(-U) \tag{7}$$

Here U is the energy of the image. Consider only interaction between neighboring sites of the image, we have

$$U \propto \sum_{(x,y) \text{ and } (x',y') \text{ are neighbor pixels}} g(u(x,y) - u(x',y')) \propto \sum g(\nabla u) \tag{8}$$

Here $g(x)$ is a positive definite function. $P(u_0|u)$ is assumed to have the following form

$$P(u_0|u) \propto \prod_{i=1}^{N} \exp[-(u_0(i) - u(i))^2] \propto \exp[-\int (u_0 - u)^2 dxdy]. \tag{9}$$

Here i is the index of a pixel and N is the total number of pixels in the image. Thus, $P(u_0|u)$ increases as u approaches u_0. If we assume that $P(u|u_0) = \exp(-E(u, u_0))$. Then we have [28, 38, 39, 40]

$$E(u, u_0) = \int (u - u_0)^2 dxdy + \mu \int g(\nabla u) dxdy. \tag{10}$$

If we also include the boundary energy in Eq.(10), we have

$$E(u, u_0) = \int (u - u_0)^2 dxdy + \mu \int g(\nabla u) dxdy + \nu |C|. \tag{11}$$

This is the Mumford-Shah model for $g(x) = x^2$.

The solution to the above problem for arbitrary image is not a trivial task. Therefore, many approximations and simplified models have been proposed. For segmentation problem, the most important factors are the boundaries. The texture's information inside the boundaries is not important. As the first approximation, we can take u as a constant in each region. This is called piecewise constant model and is widely used in image segmentation.

2.3 Piecewise constant approximation

If we assume that $u = c$ and c is a constant in each bounded region, then the second term in Eq.(5) is zero. Therefore, Eq.(5) becomes

$$\begin{aligned} inf_{c,C}\{E(u, C) &= \alpha \int_{\Omega \setminus C} (c - u_0)^2 dxdy + \nu |C|\} \\ &= \alpha \sum_{i=1}^{n} \int_{\Omega_i} (c_i - u_0)^2 dxdy + \nu |C|\}. \end{aligned} \tag{12}$$

If we choose $n = 2$ in Eq.(12), we will have two different values c_1 and c_2 for two different regions. We will call each region which has a different value c_i as one phase. Thus, Eq.(12) for $n = 2$ is referred as two phases MS model. This model was first used by Chan and Vese [23, 24, 22, 46]. In this simplified version of Eq.(12), the number of phases is chosen in advance. In this study, we will concentrate first on the two phase problem. We will later extend this study to four phases based on our previous work [8, 9].

Using the Heaviside function $H(x)$ defined as

$$H(x) = \left\{ \begin{array}{l} 1 \text{ if } x > 0 \\ 0 \text{ if } x < 0 \end{array} \right\} \tag{13}$$

and the level set function $\phi(x, y)$

$$\phi(x) \quad \left\{ \begin{array}{l} > 0 \text{ if } (x, y) in \Omega \\ = 0 \text{ if } (x, y) in \delta\Omega \\ < 0 \text{ if } (x, y) in \bar{\Omega} \end{array} \right\}, \tag{14}$$

the two phase version of Eq.(12) can be written as

$$\begin{aligned} E(u, C) &= \alpha \int_{inside\ C} (c_1 - u_0)^2 dxdy + \alpha \int_{outside\ C} (c_2 - u_0)^2 dxdy + \nu |C| \\ &= \alpha \int (c_1 - u_0)^2 H(\phi) dx\ dy + \alpha (c_2 - u_0)^2 (1 - H(\phi)) dxdy \\ &\quad + \nu \int |\nabla H(\phi)| dxdy. \end{aligned} \tag{15}$$

Since $\nabla H(\phi)$ is nonzero only on the boundary of the curve, therefore the length term can be written as

$$length(\delta\Omega) = \int |\nabla H(\phi)| dxdy \tag{16}$$

and this has been used in Eq.(15).

Using the formula

$$\nabla H(\phi) = \delta(\phi) \nabla \phi, \tag{17}$$

We have

$$length(\delta\Omega) = \int |\nabla H(\phi)| dxdy = \int_{\Omega} \delta(\phi) |\nabla \phi| dxdy. \tag{18}$$

with

$$|\nabla \phi| = \sqrt{\phi_x^2 + \phi_y^2}. \tag{19}$$

Eq.(18) will be used in the latter part of this chapter.

If we define:

$$F(\phi) = \alpha(c_1 - u_0)^2 H(\phi) + \alpha(c_2 - u_0)^2(1 - H(\phi)) + \nu\delta(\phi)|\nabla\phi| \tag{20}$$

and follow the derivation given in Appendix A, we have

$$\frac{\partial F}{\partial \phi} = \alpha(c_1 - u_0)^2\delta(\phi) - \alpha(c_2 - u_0)^2\delta(\phi)) + \nu[\delta'(\phi)|\nabla\phi|] \tag{21}$$

and

$$\frac{\partial}{\partial y}(\frac{\partial F}{\partial \phi_x}) = \nu[\delta'(\phi)\frac{\phi_x^2}{\sqrt{\phi_x^2 + \phi_y^2}} + \delta(\phi)\frac{\partial}{\partial x}\frac{\phi_x}{\sqrt{\phi_x^2 + \phi_y^2}}] \tag{22}$$

and

$$\frac{\partial}{\partial y}(\frac{\partial F}{\partial \phi_y}) = \nu[\delta'(\phi)\frac{\phi_y^2}{\sqrt{\phi_x^2 + \phi_y^2}} + \delta(\phi)\frac{\partial}{\partial y}\frac{\phi_y}{\sqrt{\phi_x^2 + \phi_y^2}}] \tag{23}$$

Thus, we have the following Euler-Lagrange equation:

$$\delta(\phi)[\alpha(c_1 - u_0)^2 - \alpha(c_2 - u_0)^2 - \nu\nabla \cdot (\frac{\nabla\phi}{|\nabla\phi}|)] = 0 \tag{24}$$

with the boundary condition (see Appendix A)

$$\frac{\delta(\phi)}{|\nabla\phi|}\nabla\phi \cdot \hat{n} = \frac{\delta(\phi)}{|\nabla\phi|}\frac{\partial\phi}{\partial n} = 0. \tag{25}$$

Here $\hat{n}$ is the normalized normal of the boundary curve of the image.

In the following, we will denote the LHS of Eq.(24) by $L(\phi)$. Using the gradient projection method, we can change Eq.(24) to the following time dependent equation

$$\frac{\partial\phi}{\partial t} = -L(\phi) = \delta(\phi)[-\alpha(c_1 - u_0)^2 + \alpha(c_2 - u_0)^2 + \nu\nabla \cdot (\frac{\nabla\phi}{|\nabla\phi}|)]. \tag{26}$$

In the following, we will prove that $\frac{\partial E}{\partial t} \leq 0$. That is the solution of Eq.(26) will decrease $E(c_i, C)$ in time. Therefore the final solution of Eq.(26) should minimize the function $E(c_i, C)$.

From Eq.(15), we have

$$\begin{aligned}\frac{\partial E(c_i,C)}{\partial t} &= \int[\alpha(c_1-u_0)^2\delta(\phi)\frac{\partial\phi}{\partial t}-\alpha(c_2-u_0)^2\delta(\phi)\frac{\partial\phi}{\partial t}]dxdy \\ &+\nu\int\frac{\partial\delta(\phi)}{\partial\phi}\frac{\partial\phi}{\partial t}|\nabla(\phi)|dxdy+\nu\int\delta(\phi)\frac{\partial|\nabla(\phi)|}{\partial\phi_x}\frac{\partial\phi_x}{\partial t}dxdy \\ &+\nu\int\delta(\phi)\frac{\partial|\nabla(\phi)|}{\partial\phi_y}\frac{\partial\phi_y}{\partial t}dxdy \end{aligned} \tag{27}$$

Using the fact that

$$\frac{\partial\phi_y}{\partial t}=\frac{\partial(\frac{\partial\phi}{\partial t})}{\partial y},\qquad \frac{\partial\phi_x}{\partial t}=\frac{\partial(\frac{\partial\phi}{\partial t})}{\partial x} \tag{28}$$

Then Eq.(27) becomes:

$$\begin{aligned}\frac{\partial E(c_i,C)}{\partial t} &= \int[\alpha(c_1-u_0)^2\delta(\phi)\frac{\partial\phi}{\partial t}-\alpha(c_2-u_0)^2\delta(\phi)\frac{\partial\phi}{\partial t}]dxdy \\ &+\nu\int\frac{\partial\delta(\phi)}{\partial\phi}\frac{\partial\phi}{\partial t}|\nabla(\phi)|dxdy \\ &+\nu\int\nabla\cdot(\vec{B}\frac{\partial\phi}{\partial t})dxdy-\nu\int(\nabla\cdot\vec{B})\frac{\partial\phi}{\partial t}dxdy \end{aligned} \tag{29}$$

with

$$\vec{B}=\delta(\phi)(\frac{\partial|\nabla\phi|}{\partial\phi_x},\frac{\partial|\nabla\phi|}{\partial\phi_y})=\delta(\phi)\frac{\nabla\phi}{|\nabla\phi|}. \tag{30}$$

Because the boundary condition of the Euler-Lagrange equation

$$\int\nabla\cdot\vec{B}dxdy=\int\vec{B}\cdot\vec{n}dl=0, \tag{31}$$

and

$$\nabla\cdot\vec{B}=\delta'(\phi)|\nabla\phi|+\delta(\phi)\nabla\cdot\frac{\nabla\phi}{|\nabla\phi|}, \tag{32}$$

we have

$$\begin{aligned}\frac{\partial E(c_i,C)}{\partial t} &= -\int\left\{\delta(\phi)[\alpha(c_1-u_0)^2+\alpha(c_2-u_0)^2-\nu\nabla\cdot(\frac{\nabla\phi}{|\nabla\phi}))]\right\}^2dxdy \\ &= -\int L(\phi)^2dxdy\le 0. \end{aligned} \tag{33}$$

Thus we have shown in Eq.(33) that $\frac{\partial E}{\partial t} \leq 0$. In Appendix B, we show that this result is true for any kind of Lagrangian.

For a fixed ϕ, using the assumption that c_1 and c_2 are constants, we have

$$\frac{\partial E}{\partial c_1} = 0, \quad \frac{\partial E}{\partial c_2} = 0. \tag{34}$$

Thus

$$c_1(\phi) = \frac{\int u_0 H(\phi) dxdy}{\int H(\phi) dxdy}, \tag{35}$$

and

$$c_2(\phi) = \frac{\int u_0 (1 - H(\phi)) dxdy}{\int (1 - H(\phi)) dxdy}. \tag{36}$$

In numerical calculations, we use

$$H_\epsilon(x) = \frac{1}{2}(1 + \frac{2}{\pi} \arctan(\frac{x}{\epsilon})) \tag{37}$$

and

$$\delta_\epsilon(x) = \frac{1}{\pi} \frac{\epsilon}{x^2 + \epsilon^2} \tag{38}$$

to replace $H(\phi)$ and $\delta(\phi)$. In Fig. 2, H_ϵ and δ_ϵ are shown for two different ϵ values. The smaller the ϵ is, the closer $H_\epsilon(x)$ and $\delta_\epsilon(x)$ are to $H(x)$ and $\delta(x)$. If $\epsilon \to 0$, $H(x)$ and $\delta(x)$ are regained.

2.4 Experimental results using the two-phase piecewise constant model

In Fig. 3, the piecewise constant approximation is used to segment a Chinese character. It is seen that the segmentation result is very good. The steps of the segmentation are also shown in Fig. 3. It is clear that after 3 iterations, the boundary of the Chinese character is found. The energy changes with time is shown in Fig. 4. The numerical results confirm that as time goes on, the total energy decreases and reaches a constant value when time becomes very large. Fig. 4 is consistent with the results shown in Fig. 3. In the calculations in this section, we fix $\nu = 0.05\sigma^2$ and σ^2 is the variation of the input image.

In Figs. 5 and 6, the segmentation results of David picture and some geometrical

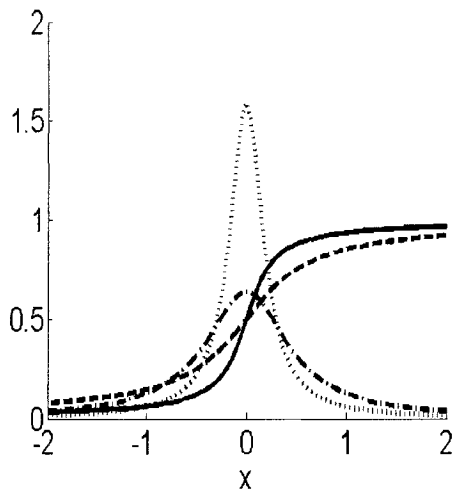

Figure 2: $H_\epsilon(x)$ *and* $\delta_\epsilon(x)$ *are shown in the figure. Solid line corresponds to* $H_\epsilon(x)$ *for* $\epsilon = 0.2$. *The dashed line corresponds to* $H_\epsilon(x)$ *for* $\epsilon = 0.5$. *The doted line corresponds to* $\delta_\epsilon(x)$ *for* $\epsilon = 0.2$ *and The dot-dash line corresponds to* $\delta_\epsilon(x)$ *for* $\epsilon = 0.5$

shapes are shown. It is clear that the piecewise constant can detect the boundary of objects in the image. The total energy decreases vs. time (iterations) and this confirms again our derivation in this chapter.

In Figs. 7 and Fig. 8, the segmentation results of an astronomy image and an artificial image are shown. They both give good segmentation results.

The two phase Mumford-Shah model can not detect tri-junction regions as shown in Fig. 9. In (a) of Fig. 9, we have three different regions, but the two-phase Mumford-Shah model always misses one region as shown in (b) of Fig. 9. This is easy to understand. Since we have only two phases, so two adjacent regions must be in the same phase. Therefore, we can not detect the three different regions in (a). To overcome this problem, we need to use more level sets. If we have two level sets, then the whole image can be divided into four regions. Thus using two level sets, we can detect tri-junction. If we have n level sets, then we have 2^n phases. In the following section, we will study two level sets Mumford-Shah model.

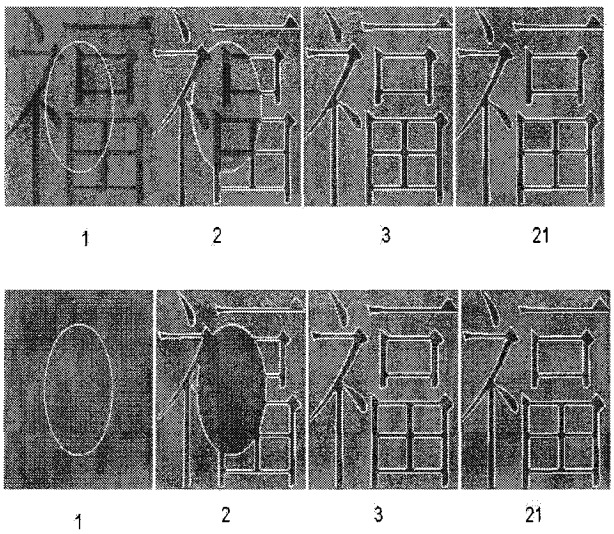

Figure 3: *Segmentation results of a Chinese character "fu" (blessing). After* 21 *iterations, we get the final result. The evolution of the level set with time (iterations) is also shown.*

2.5 The four-phase piecewise constant Mumford-Shah model

For two level set functions ϕ_1, ϕ_2, the total image can be divided into four regions as shown in Fig. 10. Using $H(\phi_1)$ and $H(\phi_2)$, the four-phase Mumford-Shah model can be written as

$$\begin{aligned}
&E_4(c_{11}, c_{01}, c_{10}, c_{00}, \phi_1, \phi_2) = \\
&\int [(u_0 - c_{11})^2 H(\phi_1)H(\phi_2) + (u_0 - c_{10})^2 H(\phi_1)(1 - H(\phi_2)) \\
&+(u_0 - c_{01})^2 (1 - H(\phi_1))H(\phi_2) + (u_0 - c_{00})^2 (1 - H(\phi_1))(1 - H(\phi_2))]dxdy \\
&+\nu \int |\nabla H(\phi_1)|dxdy. + \nu \int |\nabla H(\phi_2)|dxdy. \qquad (39)
\end{aligned}$$

Let

$$\begin{aligned}
F_4(\phi_1, \phi_2) \;=\; & (u_0 - c_{11})^2 H(\phi_1)H(\phi_2) + (u_0 - c_{10})^2 H(\phi_1)(1 - H(\phi_2)) \\
& +(u_0 - c_{01})^2 (1 - H(\phi_1))H(\phi_2) + (u_0 - c_{00})^2 (1 - H(\phi_1))(1 - H(\phi_2)) \\
& +\nu|\nabla H(\phi_1)| + \nu|\nabla H(\phi_2)| \qquad (40)
\end{aligned}$$

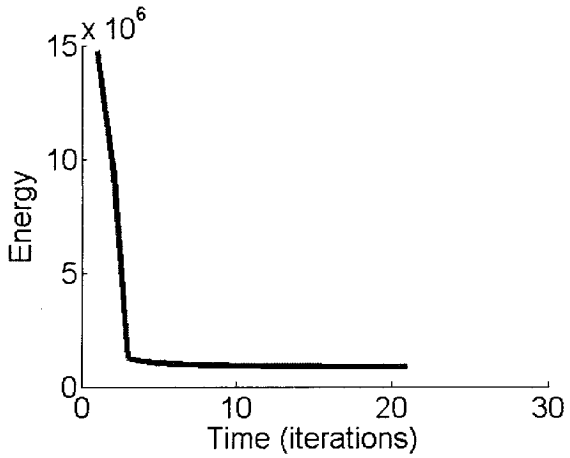

Figure 4: *The Mumford-Shah energy changes with time.*

we have

$$\begin{aligned}\frac{\partial F_4}{\partial \phi_1} &= (c_{11}-u_0)^2\delta(\phi_1)H(\phi_2)+(c_{10}-u_0)^2\delta(\phi_1)(1-H(\phi_2)) \\ &\quad -(c_{01}-u_0)^2\delta(\phi_1)H(\phi_2)-(c_{00}-u_0)^2\delta(\phi_1)(1-H(\phi_2)) \\ &\quad +\nu\delta'(\phi_1)|\nabla\phi_1| \end{aligned} \tag{41}$$

and

$$\frac{\partial}{\partial x}\left(\frac{\partial F_4}{\partial \phi_{1x}}\right) = \nu\left[\delta'(\phi_1)\frac{\phi_{1x}^2}{\sqrt{\phi_{1x}^2+\phi_{1y}^2}}+\delta(\phi_1)\frac{\partial}{\partial x}\frac{\phi_{1x}}{\sqrt{\phi_{1x}^2+\phi_{1y}^2}}\right] \tag{42}$$

and

$$\frac{\partial}{\partial y}\left(\frac{\partial F_4}{\partial \phi_{1y}}\right) = \nu\left[\delta'(\phi_1)\frac{\phi_{1y}^2}{\sqrt{\phi_{1x}^2+\phi_{1y}^2}}+\delta(\phi_1)\frac{\partial}{\partial y}\frac{\phi_{1y}}{\sqrt{\phi_{1x}^2+\phi_{1y}^2}}\right] \tag{43}$$

Therefore, we have the following Euler-Lagrange equation for ϕ_1:

$$\begin{aligned}&\delta(\phi_1)\Big[[(c_{11}-u_0)^2-(c_{01}-u_0)^2]H(\phi_2)+ \\ &[(c_{10}-u_0)^2-(c_{00}-u_0)^2](1-H(\phi_2))-\nu\nabla\cdot\left(\frac{\nabla\phi_1}{|\nabla\phi_1}\right)\Big]=0\end{aligned} \tag{44}$$

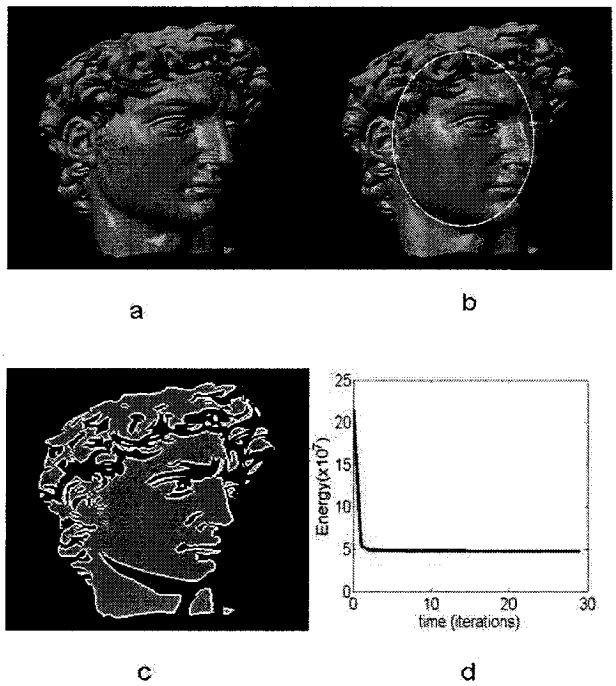

Figure 5: *Segmentation results of the David image.* (a) : *the original image,* (b) : *the initial level set,* (c) : *the final segmentation results,* (d) : *the MS energy vs time (iterations).*

with the boundary condition (see Appendix A)

$$\frac{\delta(\phi_1)}{|\nabla\phi_1|}\nabla\phi_1 \cdot \hat{n} = \frac{\delta(\phi_1)}{|\nabla\phi_1|}\frac{\partial\phi_1}{\partial n} = 0. \tag{45}$$

Here $\hat{n}$ is the normalized normal of the boundary curve of the image.

Similarly, we can derive the Euler-Lagrangian equation for ϕ_2.

$$\begin{aligned}\frac{\partial F_4}{\partial\phi_2} &= (c_{11}-u_0)^2\delta(\phi_2)H(\phi_1) - (c_{10}-u_0)^2H(\phi_1)\delta(\phi_2) \\ &\quad +(c_{01}-u_0)^2\delta(\phi_2)(1-H(\phi_1)) - (c_{00}-u_0)^2(1-H(\phi_1))\delta(\phi_2) \\ &\quad +\nu[\delta'(\phi_2)|\nabla\phi_1|\end{aligned} \tag{46}$$

and

$$\frac{\partial}{\partial x}\left(\frac{\partial F_4}{\partial\phi_{2x}}\right) = \nu[\delta'(\phi_2)\frac{\phi_{2x}^2}{\sqrt{\phi_{2x}^2+\phi_{2y}^2}} + \delta(\phi_2)\frac{\partial}{\partial x}\frac{\phi_{2x}}{\sqrt{\phi_{2x}^2+\phi_{2y}^2}}] \tag{47}$$

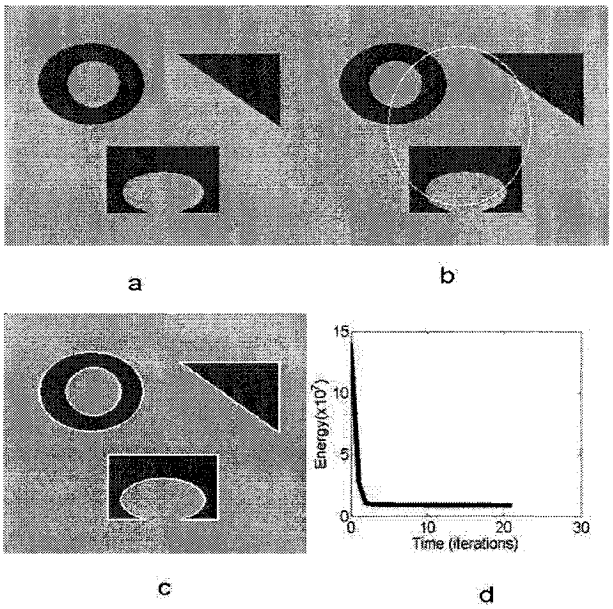

Figure 6: *Segmentation results of a image.* (a) : *the original image,* (b) : *the initial level set,* (c) : *the final segmentation results,* (d) : *the MS energy vs time (iterations).*

and

$$\frac{\partial}{\partial y}(\frac{\partial F_4}{\partial \phi_{2y}}) = \nu[\delta'(\phi_2)\frac{\phi_{2y}^2}{\sqrt{\phi_{2x}^2+\phi_{2y}^2}} + \delta(\phi_2)\frac{\partial}{\partial y}\frac{\phi_{2y}}{\sqrt{\phi_{2x}^2+\phi_{2y}^2}}] \tag{48}$$

Therefore, we have the following Euler-Lagrange equation for ϕ_2:

$$\begin{aligned}&\delta(\phi_2)\Big[[(c_{11}-u_0)^2-(c_{10}-u_0)^2]H(\phi_1)+\\&[(c_{01}-u_0)^2-(c_{00}-u_0)^2](1-H(\phi_1))-\nu\nabla\cdot(\frac{\nabla\phi_2}{|\nabla\phi_2}|)\Big]=0\end{aligned} \tag{49}$$

with the boundary condition(see Appendix A)

$$\frac{\delta(\phi_2)}{|\nabla\phi_2|}\nabla\phi_2\cdot\hat{n}=\frac{\delta(\phi_2)}{|\nabla\phi_2|}\frac{\partial\phi_2}{\partial n}=0. \tag{50}$$

Here $\hat{n}$ is the normalized normal of the boundary curve of the image.

We need to notice that Eq.(44) and Eq.(49) are two coupled equations. We will denote the LHS of Eq.(44) and Eq.(49) as $L_1(\phi_1,\phi_2)$ and $L_2(\phi_1,\phi_2)$ respectively.

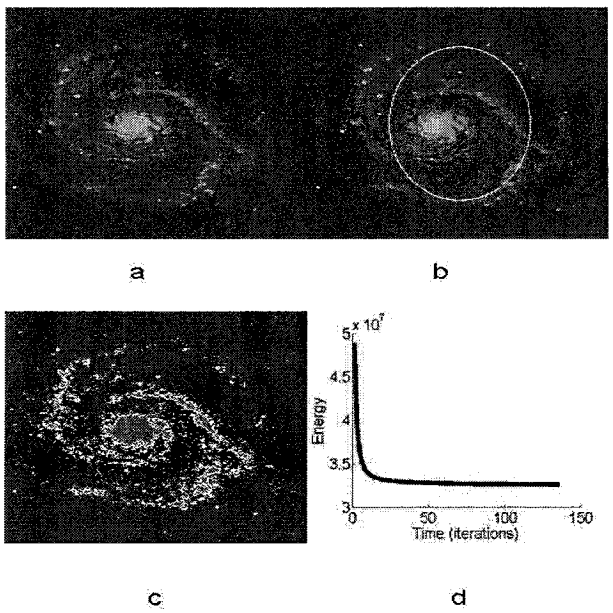

Figure 7: *Segmentation results of a galaxy image.* (a) : *the original image,* (b) : *the initial level set,* (c) : *the segmentation results,* (d) : *energy vs. time (iterations).*

Using the gradient projection method, we have the following equations:

$$\frac{\partial \phi_1}{\partial t} = -L_1 \qquad \frac{\partial \phi_2}{\partial t} = -L_2 \tag{51}$$

In the following, we want to prove that the $\frac{\partial E_4}{\partial t} \leq 0$.

From Eq.(39), we have

$$\begin{aligned}
\frac{\partial E_4}{\partial t} &= \int (c_{11} - u_0)^2 [\delta(\phi_1)\frac{\partial \phi_1}{\partial t} H(\phi_2) + H(\phi_1)\delta(\phi_2)\frac{\partial \phi_2}{\partial t}] dxdy \\
&+ \int (c_{10} - u_0)^2 [\delta(\phi_1)\frac{\partial \phi_1}{\partial t}(1 - H(\phi_2) - H(\phi_1)\delta(\phi_2)\frac{\partial \phi_2}{\partial t}] dxdy \\
&+ \int (c_{01} - u_0)^2 [-\delta(\phi_1)\frac{\partial \phi_1}{\partial t} H(\phi_2) + (1 - H(\phi_1))\delta(\phi_2)\frac{\partial \phi_2}{\partial t}] dxdy \\
&+ \int (c_{00} - u_0)^2 [-\delta(\phi_1)\frac{\partial \phi_1}{\partial t}(1 - H(\phi_2)) - (1 - H(\phi_1))\delta(\phi_2)\frac{\partial \phi_2}{\partial t}] dxdy \\
&+ \nu \int \frac{\partial \delta(\phi_1)}{\partial \phi_1}\frac{\partial \phi_1}{\partial t}|\nabla(\phi_1)| dxdy + \nu \int \delta(\phi_1)\frac{\partial |\nabla(\phi_1)|}{\partial \phi_{1x}}\frac{\partial \phi_{1x}}{\partial t} dxdy \\
&+ \nu \int \delta(\phi_1)\frac{\partial |\nabla(\phi_1)|}{\partial \phi_{1y}}\frac{\partial \phi_{1y}}{\partial t} dxdy \\
&+ \nu \int \frac{\partial \delta(\phi_2)}{\partial \phi_2}\frac{\partial \phi_2}{\partial t}|\nabla(\phi_2)| dxdy + \nu \int \delta(\phi_2)\frac{\partial |\nabla(\phi_2)|}{\partial \phi_{2x}}\frac{\partial \phi_{2x}}{\partial t} dxdy
\end{aligned}$$

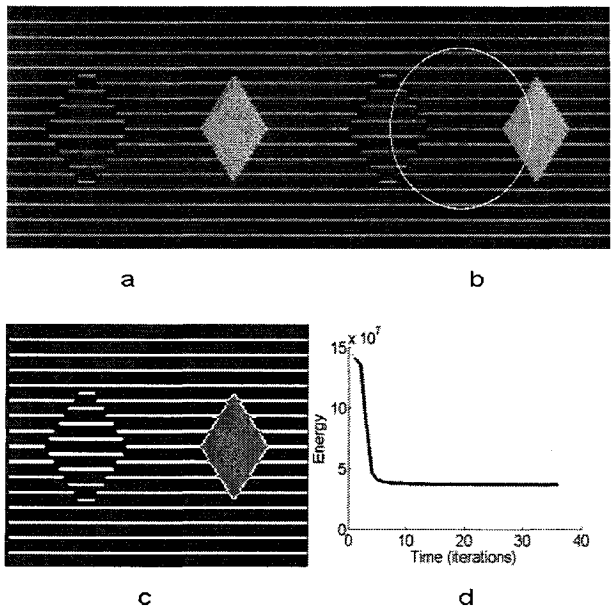

Figure 8: *Segmentation results of a image.* (a) : *the original image,* (b) : *the initial level set,* (c) : *the segmentation results,* (d) : *energy vs. time (iterations).*

$$+\nu \int \delta(\phi_2) \frac{\partial |\nabla(\phi_2)|}{\partial \phi_{2y}} \frac{\partial \phi_{2y}}{\partial t} dxdy \tag{52}$$

Using the fact that

$$\frac{\partial \phi_{1y}}{\partial t} = \frac{\partial (\frac{\partial \phi_1}{\partial t})}{\partial y} \qquad \frac{\partial \phi_{1x}}{\partial t} = \frac{\partial (\frac{\partial \phi_1}{\partial t})}{\partial x} \tag{53}$$

and

$$\frac{\partial \phi_{2y}}{\partial t} = \frac{\partial (\frac{\partial \phi_2}{\partial t})}{\partial y} \qquad \frac{\partial \phi_{2x}}{\partial t} = \frac{\partial (\frac{\partial \phi_2}{\partial t})}{\partial x} \tag{54}$$

Then Eq.(52) becomes:

$$\begin{aligned}
\frac{\partial E_4(u,C)}{\partial t} &= \int (c_{11}-u_0)^2 [\delta(\phi_1)\frac{\partial \phi_1}{\partial t} H(\phi_2) + H(\phi_1)\delta(\phi_2)\frac{\partial \phi_2}{\partial t}] dxdy \\
&+ \int (c_{10}-u_0)^2 [\delta(\phi_1)\frac{\partial \phi_1}{\partial t}(1-H(\phi_2)) - H(\phi_1)\delta(\phi_2)\frac{\partial \phi_2}{\partial t}] dxdy \\
&+ \int (c_{01}-u_0)^2 [-\delta(\phi_1)\frac{\partial \phi_1}{\partial t} H(\phi_2) + (1-H(\phi_1))\delta(\phi_2)\frac{\partial \phi_2}{\partial t}] dxdy \\
&+ \int (c_{00}-u_0)^2 [-\delta(\phi_1)\frac{\partial \phi_1}{\partial t}(1-H(\phi_2)) - (1-H(\phi_1))\delta(\phi_2)\frac{\partial \phi_2}{\partial t}] dxdy \\
&+ \nu \int \delta'(\phi_1)|\nabla \phi_1| \frac{\partial \phi_1}{\partial t} dxdy + \nu \int \delta'(\phi_2)|\nabla \phi_2| \frac{\partial \phi_2}{\partial t} dxdy
\end{aligned}$$

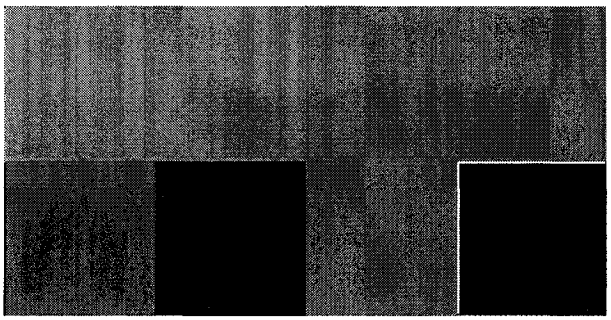

a b

Figure 9: *One level set results for a tri-junction region. (a) is the original image and (b) is the segmentation result.*

$$+\nu \int \nabla \cdot (\vec{B_1} \frac{\partial \phi_1}{\partial t}) dxdy - \nu \int (\nabla \cdot \vec{B_1}) \frac{\partial \phi_1}{\partial t} dxdy$$
$$+\nu \int \nabla \cdot (\vec{B_2} \frac{\partial \phi_2}{\partial t}) dxdy - \nu \int (\nabla \cdot \vec{B_2}) \frac{\partial \phi_2}{\partial t} dxdy \tag{55}$$

with

$$\vec{B_1} = \delta(\phi_1)(\frac{\partial |\nabla \phi_1|}{\partial \phi_{1x}}, \frac{\partial |\nabla \phi_1|}{\partial \phi_{1y}}) = \delta(\phi_1) \frac{\nabla \phi_1}{|\nabla \phi_1|}. \tag{56}$$

and

$$\vec{B_2} = \delta(\phi_2)(\frac{\partial |\nabla \phi_2|}{\partial \phi_{2x}}, \frac{\partial |\nabla \phi_2|}{\partial \phi_{2y}}) = \delta(\phi_2) \frac{\nabla \phi_2}{|\nabla \phi_2|}. \tag{57}$$

Because of the boundary condition of the Euler-Lagrange equation

$$\int \nabla \cdot \vec{B_1} dxdy = \int \vec{B_1} \cdot \vec{n} dl = 0 \qquad \int \nabla \cdot \vec{B_2} dxdy = \int \vec{B_2} \cdot \vec{n} dl = 0, \tag{58}$$

$$\nabla \cdot \vec{B_1} = \delta'(\phi_1) |\nabla \phi_1| + \delta(\phi_1) \nabla \cdot \frac{\nabla \phi_1}{|\nabla \phi_1|}, \tag{59}$$

and

$$\nabla \cdot \vec{B_2} = \delta'(\phi_2) |\nabla \phi_2| + \delta(\phi_2) \nabla \cdot \frac{\nabla \phi_2}{|\nabla \phi_2|}, \tag{60}$$

we have

$$\begin{aligned} \frac{\partial E(u,C)}{\partial t} &= -\int \Big\{ \delta(\phi_1) \Big[[-(c_{11}-u_0)^2 + (c_{01}-u_0)^2] H(\phi_2) + \\ &\quad [(c_{10}-u_0)^2 - (c_{00}-u_0)^2](1-H(\phi_2)) + \nu \frac{\nabla \phi_1}{|\nabla \phi_1|} \Big] \Big\}^2 \end{aligned}$$

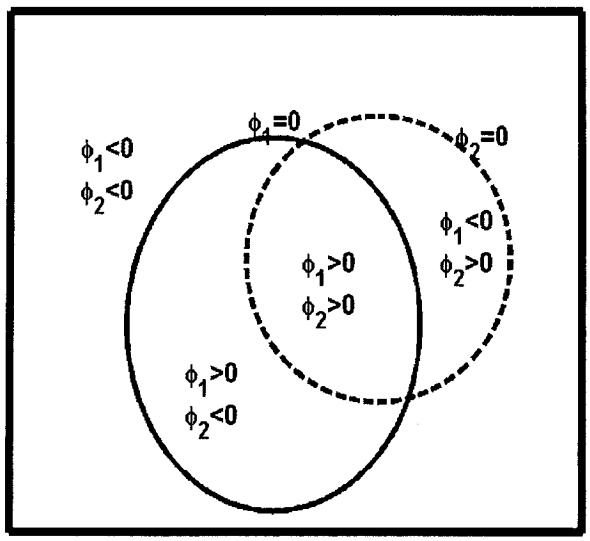

Figure 10: *Illustration of two level sets. The whole image is divided into four regions. The mean value in the region* $\phi_1 > 0, \phi_2 > 0$ *is* c_{11}. *The mean value in the region* $\phi_1 > 0, \phi_2 < 0$ *is* c_{10}. *The mean value in the region* $\phi_1 < 0, \phi_2 > 0$ *is* c_{01}. *The mean value in the region* $\phi_1 < 0, \phi_2 < 0$ *is* c_{00}.

$$
\begin{aligned}
& -\int \Big\{\delta(\phi_2)\Big[[-(c_{11}-u_0)^2+(c_{01}-u_0)^2]H(\phi_1)+[(c_{10}-u_0)^2-(c_{00}-u_0)^2] \\
& (1-H(\phi_1))+\nu\frac{\nabla\phi_2}{|\nabla\phi_2|}\Big]\Big\}^2 \\
= \; & -\int (L_1^2+L_2^2)dxdy \leq 0
\end{aligned} \tag{61}
$$

Eq.(61) is generally true for arbitrary Lagrangian. The derivation can be found in Appendix B.

The shortcoming of two level set method is that it depends strongly on the initial conditions. This can be seen from Fig. 11 where the total MS energy is calculated for different initial conditions. It is clear that the final energies are different for the two different initial conditions. Therefore, we should be very careful in choosing the initial conditions when using the two level sets. To overcome this difficult, a hierarchical multiphase segmentation method is suggested in Ref. [8]. This method has the advantage that its segmentation results do not depend on the initial conditions.

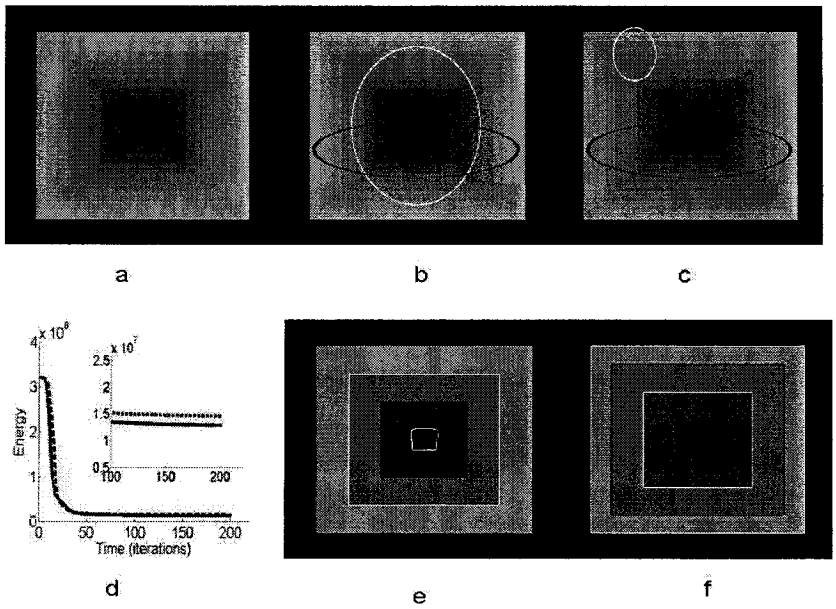

Figure 11: *Illustration of segmentation results of two level set method.* (a) : *the original image,* (b) : *initial curves of two level sets,* (c) : *different initial curves of two level sets,* (e) : *the segmentation results of b,* (f) : *the segmentation results of c,* (d) : *energy vs. time (iterations). The two segmentation results have different final MS energy. This shows clearly in top right corner of the* (d) *which is the plot for the number of iterations between* 100 *and* 200 *using different scale.*

2.6 The hierarchical multiphase segmentation method

Since the two level sets method depends on the initial conditions, in [8] the hierarchical multiphase method was introduced. At the first stage, we apply the constant MS segmentation model with one level set function ϕ_1 to a given image. At the end of the first segmentation stage, we obtain two sets of resulting sub-regions. The second stage starts by applying the same model with another level set function ϕ_2 to each of the sub-regions independently. After the second segmentation, we obtain four resulting sub-sub-regions. We can apply the same model with the third level set function ϕ_3 and so on. In our calculations, we only use two level set functions. We illustrate our multiphase hierarchical approach through the case of the 4-phase (two level set functions) segmentation. Like the Chan-Vese model, there are two evolution curves C_1 and C_2, which are represented by the corresponding level set functions ϕ_1 and ϕ_2. At the first segmentation stage, the evolution of the curve C_1 is governed by

the motion equation of the level set function ϕ_1 ($\alpha = 1$):

$$\frac{\partial \phi_1}{\partial t} = \delta(\phi_1)[\nu \nabla \cdot \frac{\nabla \phi_1}{|\nabla \phi_1|} - (u_0 - c_1)^2 + (u_0 - c_2)^2] \tag{62}$$

where c_1 and c_2 are the averages of u_0 inside and outside C_1 respectively. In other words, we will calculate ϕ_1 using the one level set method. We then obtain two-regions defined by $\phi_1 > 0$ and $\phi_1 < 0$.

After the first stage, we will use one level set PDE equation for each region separately. That is for region I ($\phi_1 > 0$), we have

$$\frac{\partial \phi_2}{\partial t} = \delta(\phi_2)[\nu_1 \nabla \cdot \frac{\nabla \phi_1}{|\nabla \phi_1|} - (u_0 - c_{11})^2 + (u_0 - c_{10})^2]. \tag{63}$$

where c_{11} is the average of u_0 in sub-region I and also inside the curve C_2 ($\phi_1 > 0, \phi_2 > 0$) and c_{10} is the average of u_0 inside the sub-region I and outside the curve C_2.

For sub-region II($\phi_1 < 0$), we have

$$\frac{\partial \phi_2}{\partial t} = \delta(\phi_2)[\nu_2 \nabla \cdot \frac{\nabla \phi_1}{|\nabla \phi_1|} - (u_0 - c_{01})^2 + (u_0 - c_{00})^2]. \tag{64}$$

where c_{01} is the average of u_0 in sub-region II and also inside the curve C_2 ($\phi_1 < 0, \phi_2 > 0$) and c_{00} is the average of u_0 inside the sub-region II and outside the curve C_2. This approach corresponds to solving the one level set equation 3 times. The advantage of this method is that the results do not depend on the initial conditions.

Here we need to point out that Eq.(63) and Eq.(64) come from the second equation of Eq.(51) which is

$$\begin{aligned} \frac{\partial \phi_2}{\partial t} &= -\delta(\phi_2) \Big[[(c_{11} - u_0)^2 - (c_{10} - u_0)^2] H(\phi_1) + \\ &\quad [(c_{01} - u_0)^2 - (c_{00} - u_0)^2](1 - H(\phi_1)) - \nu \nabla \cdot (\frac{\nabla \phi_2}{|\nabla \phi_2|}) \Big]. \end{aligned} \tag{65}$$

If $\phi_1 > 0$, $H(\phi_1) = 1$ and $1 - H(\phi_1) = 0$, thus we get Eq.(63) from Eq.(65). If $\phi_1 < 0$, $H(\phi_1) = 0$ and $1 - H(\phi_1) = 1$, thus we get Eq.(64) from Eq.(65).

We have proved that using gradient projection method, we always have $\frac{\partial E}{\partial t} < 0$. This should be also true for the hierarchical method. In Fig. 12, we see that for the

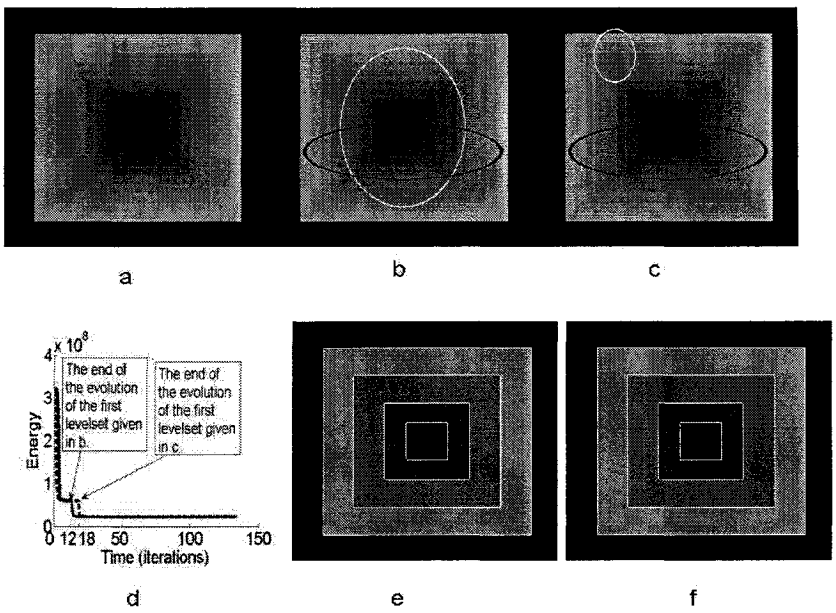

Figure 12: *Illustration of segmentation results of two level set hierarchical method.* (a) : *the original image,* (b) : *initial curves of two level sets,* (c) : *another initial curves of two level sets,* (e) : *the segmentation results of b,* (f) : *the segmentation results of c,* (d) : *the energy vs. time (iterations). The two segmentation results have the same final MS energy.*

two different initial conditions, we obtain the same segmentation results. The energy vs time (iterations) is also shown. It is shown that the final segmentation results have the same MS energy. The end of the evolution time of the first level set is also marked in Figure 12 which is 12 and 18 for the initial conditions (b) and (c) respectively.

2.7 Experimental results of hierarchical multiphase method

In Fig. 13, the one level set and the hierarchical two level set results are shown. It is clear that one level set can not detect all the regions because there are many tri-junctions inside the wheel. Two level set method can detect all structures of this image. In the calculations of this section, we take $\nu = 0.05\sigma^2$ and σ^2 is the variation of the input image, $\nu_1 = 0.05\sigma_1^2$ and $\nu_2 = 0.05\sigma_2^2$. Here σ_1^2 and σ_2^2 are the variations of the region $\phi_1 > 0$ and $\phi_2 < 0$.

In Figs. 14, 15,16 17, 18, more segmentation results are shown. It is clear that

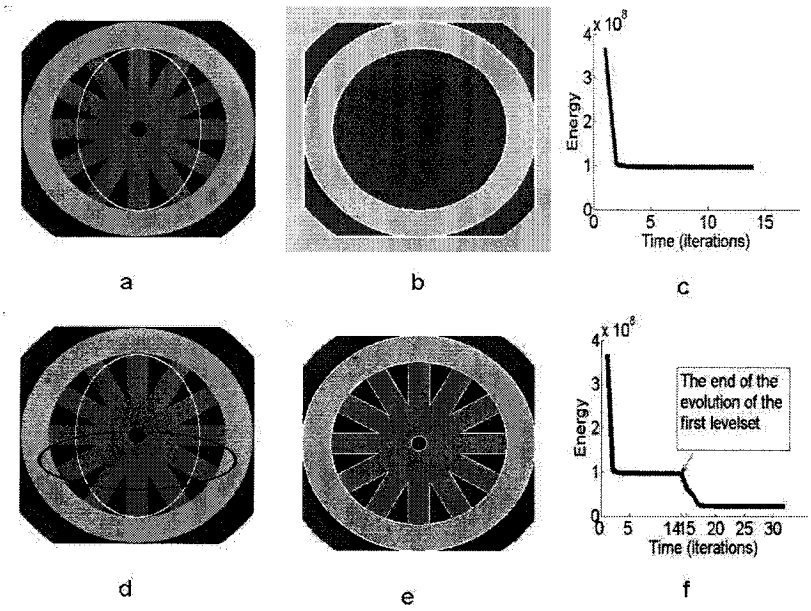

Figure 13: *Segmentation results of the hierarchical two level set method and the one level set method.* (a)*: the original image and initial level set,*(b) *: segmentation result,* (c) *: the energy vs time for one level set,* (d) *: the original image and the initial level sets,* (e) *: segmentation result,* (f) *: The MS energy vs time for hierarchical two level sets method.*

two level sets results are better than the one level set method. In (c) and (f) of those figures, the energy vs time is shown.

2.8 Conclusions and Comments

In this chapter, we have used the original MS model for image segmentation. For the first order approximation, we have assumed that u is a constant inside each of the regions. We have used the gradient projection method for solving the Euler-Lagrangian equation. The level set method was used for the numerical computations.

We have proved that the MS energy will decrease vs. time for the two-phase and four-phase approaches. In the Appendix B, we give a general proof for this statement and this should be true for arbitrary number of phases. We have shown that the hierarchical two level set method does not depend on the initial conditions.

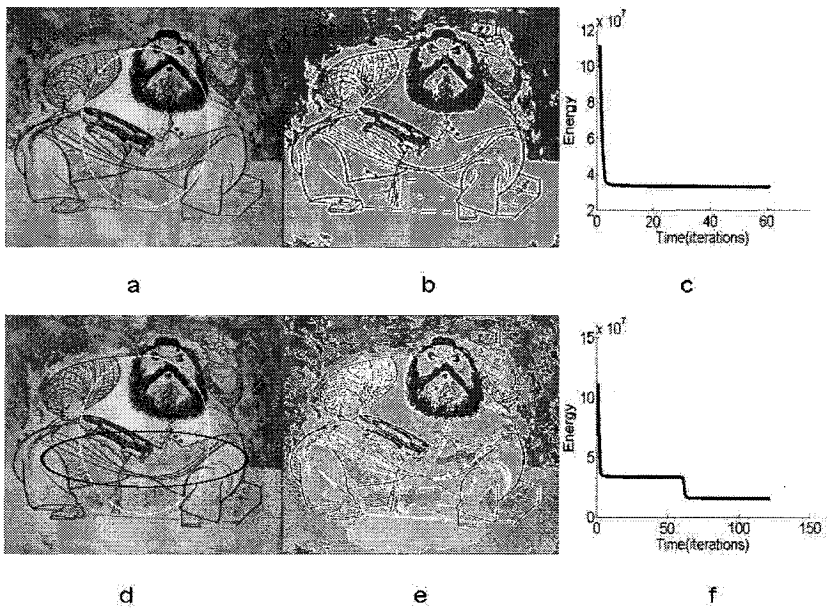

Figure 14: *Segmentation results of the hierarchical two level set method and one level set method* (a) : *the original image and initial one level set,* (b) : *the segmentation results of one level set,* (c) : *energy vs time for one level set,* (d) : *the original image and initial two level sets,* (e) : *the final segmentation results,* (f) : *the MS energy vs time for hierarchical two level sets method.*

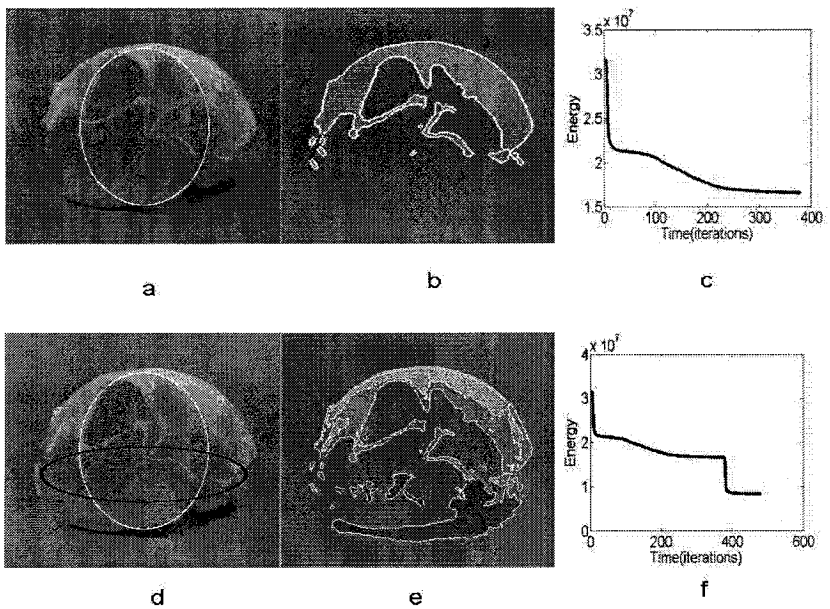

Figure 15: *Segmentation results of the hierarchical two level set method and one level set method.* (a) : *the original image and initial one level set,* (b) : *the segmentation results of one level set,* (c) : *energy vs time for one level set,* (d) : *the original image and initial two level sets,* (e) : *the final segmentation results,* (f) : *the MS energy vs time for hierarchical two level sets method.*

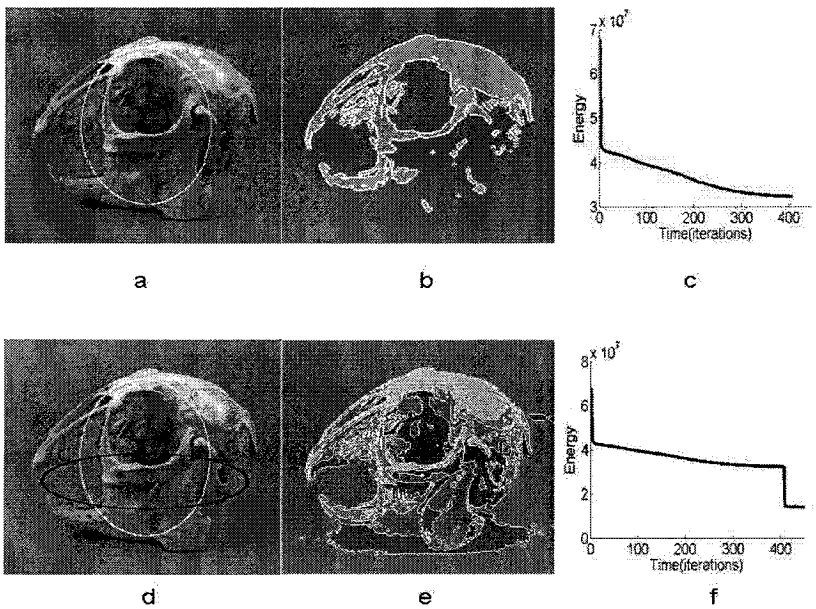

Figure 16: *Segmentation results of the hierarchical two level set method and one level set method.* (a) : *the original image and initial one level set,* (b) : *the segmentation results of one level set,* (c) : *energy vs time for one level set,* (d) : *the original image and initial two level sets,* (e) : *the final segmentation results,* (f) : *the MS energy vs time for hierarchical two level sets method.*

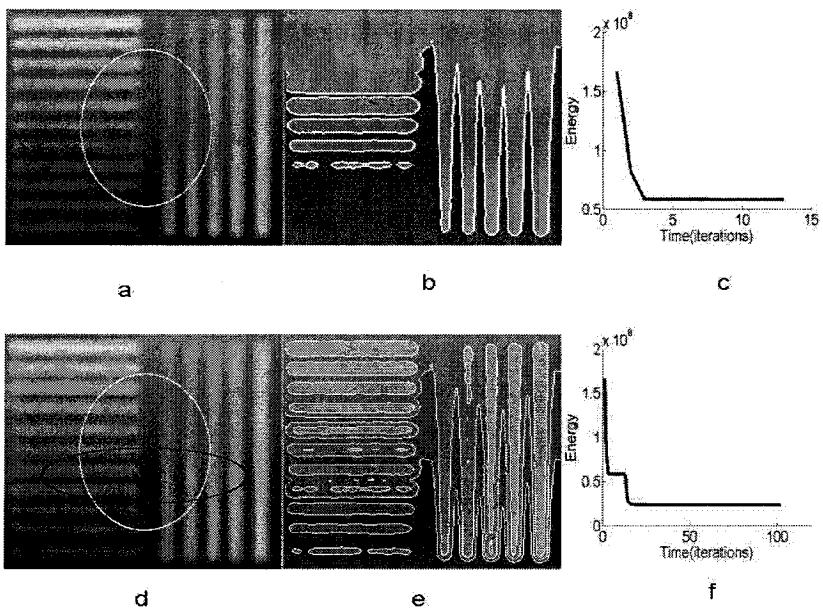

Figure 17: *Segmentation results of the hierarchical two level set method and the one level set method.* (a) : *the original image and initial one level set,* (b) : *the segmentation results of one level set,* (c) : *energy vs time for one level set,* (d) : *the original image and initial two level sets,* (e) : *the final segmentation results,* (f) : *the MS energy vs time for hierarchical two level sets method.*

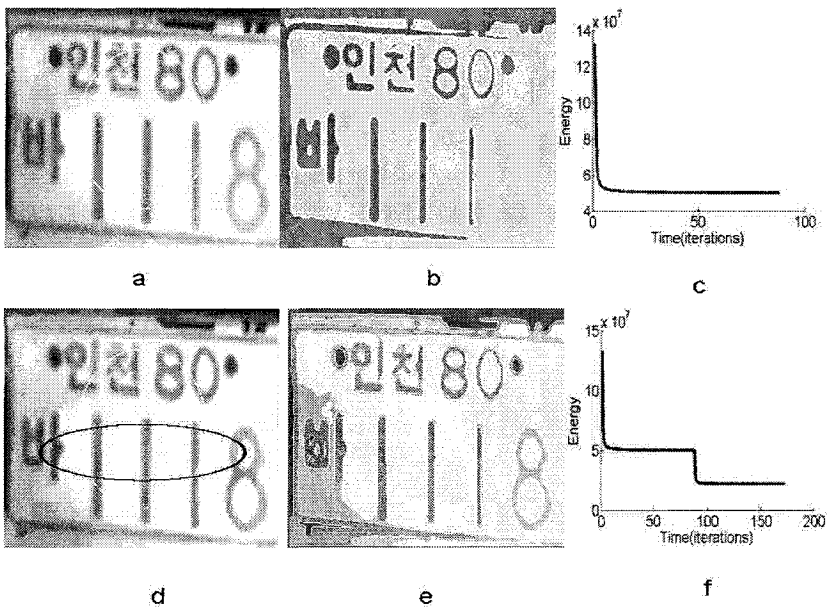

Figure 18: *Segmentation results of the hierarchical two level set method and the one level set method.* (a) : *the original image and initial one level set,* (b) : *the segmentation results of one level set,* (c) : *energy vs time for one level set,* (d) : *the original image and initial two level sets,* (e) : *the final segmentation results,* (f) : *the MS energy vs time for hierarchical two level sets method.*

Chapter 3

Linear Approximation MS Model

3.1 Introduction

In Chapter 1, we have used a piecewise constant model for image segmentation and we obtained very good results. However piecewise constant approximation may not be appropriate for images with large variations in intensities. For this kind of image, if we use constant approximation as in Chapter 1, the first term of Eq.(15) will be very large due to the large fluctuation of intensity in each region. To make the first term small, we need to have a better approximation of u_0. Therefore, instead of approximating the image in each region by a constant, we will approximate it by a planar surface [44]

$$u(x, y) = a + b \cdot x + c \cdot y. \tag{66}$$

Here a, b, c are constants.

3.2 Two-phase linear approximation

We will study two-phase linear approximation first. Later we will extend it to the case of four phases as we have done in the last chapter. For the two phase case, we will have two linear planar surfaces one approximating the inside, the other approximating the outside of the level set curve:

$$u_1(x, y) = a_1 + b_1 \cdot x + c_1 \cdot y, \tag{67}$$

and

$$u_2(x,y) = a_2 + b_2 \cdot x + c_2 \cdot y. \tag{68}$$

Eq.(4) then becomes:

$$\begin{aligned} E(a_i, b_i, c_i, C) &= \int (a_1 + b_1 x + c_1 y - u_0)^2 H(\phi) dxdy \\ &+ \int (a_2 + b_2 x + c_2 y - u_0)^2 (1 - H(\phi)) dxdy \\ &+ \mu(b_1^2 + c_1^2) \int H(\phi) dxdy + + \mu(b_2^2 + c_2^2) \int (1 - H(\phi)) dxdy + \\ &\nu \int |\nabla H(\phi)| dxdy. \end{aligned} \tag{69}$$

Let

$$\begin{aligned} F(\phi) &= (a_1 + b_1 x + c_1 y - u_0)^2 H(\phi) + (a_2 + b_2 x + c_2 y - u_0)^2 (1 - H(\phi)) \\ &+ \mu(b_1^2 + c_1^2) H(\phi) + + \mu(b_2^2 + c_2^2)(1 - H(\phi)) + \\ &+ \nu \delta(\phi) |\nabla \phi|. \end{aligned} \tag{70}$$

Following the derivation in Appendix A, we have

$$\begin{aligned} \frac{\partial F}{\partial \phi} &= (a_1 + b_1 x + c_1 y - u_0)^2 \delta(\phi) - (a_2 + b_2 x + c_2 y - u_0^2) \delta(\phi) + \\ &\mu(b_1^2 + c_1^2) \delta(\phi) - \mu(b_2^2 + c_2^2) \delta(\phi) + \nu \delta'(\phi) |\nabla \phi|] \end{aligned} \tag{71}$$

and

$$\frac{\partial}{\partial x}(\frac{\partial F}{\partial \phi_x}) = \nu[\delta'(\phi) \frac{\phi_x^2}{\sqrt{\phi_x^2 + \phi_y^2}} + \delta(\phi) \frac{\partial}{\partial x} \frac{\phi_x}{\sqrt{\phi_x^2 + \phi_y^2}}] \tag{72}$$

and

$$\frac{\partial}{\partial y}(\frac{\partial F}{\partial \phi_y}) = \nu[\delta'(\phi) \frac{\phi_y^2}{\sqrt{\phi_x^2 + \phi_y^2}} + \delta(\phi) \frac{\partial}{\partial y} \frac{\phi_y}{\sqrt{\phi_x^2 + \phi_y^2}}] \tag{73}$$

Thus, we have the following Euler-Lagrange equation:

$$\begin{aligned} &\delta(\phi)[-\nu \nabla \cdot \frac{\nabla \phi}{|\nabla \phi|} + (a_1 + b_1 x + c_1 y - u_0)^2 + \mu(b_1^2 + c_1^2) \\ &-(a_2 + b_2 x + c_2 y - u_0)^2 - \mu(b_2^2 + c_2^2)] = 0 \end{aligned} \tag{74}$$

with the following boundary condition(see Appendix A)

$$\frac{\delta(\phi)}{|\nabla\phi|}\nabla\phi\cdot\hat{n}=\frac{\delta(\phi)}{|\nabla\phi|}\frac{\partial\phi}{\partial n}=0. \tag{75}$$

Here $\hat{n}$ is the normalized normal of the boundary curve of the image. In the following we will denote the LHS of Eq.(74) by L_{linear}.

Following Appendix B, we have the time dependent evolution equation of the level set $\phi(x,y,t)$

$$\begin{aligned}\frac{\partial\phi}{\partial t} &= \delta(\phi)[\nu\nabla\cdot\frac{\nabla\phi}{|\nabla\phi|}-(a_1+b_1x+c_1y-u_0)^2-\mu(b_1^2+c_1^2)\\ &\quad+(a_2+b_2x+c_2y-u_0)^2+\mu(b_2^2+c_2^2)]\end{aligned} \tag{76}$$

We can calculate a_1, b_1, c_1 by the following equations

$$\frac{\partial E}{\partial a_1}=0,\frac{\partial E}{\partial b_1}=0,\frac{\partial E}{\partial c_1}=0. \tag{77}$$

From Eq.(77) we have

$$\begin{aligned}&a_1\int H(\phi)dxdy+b_1\int H(\phi)xdxdy\\ &+c_1\int yH(\phi)dxdy=\int u_0H(\phi)dxdy\\ &a_1\int xH(\phi)dxdy+b_1\int[x^2+\mu]H(\phi)dxdy\\ &+c_1\int xyH(\phi)dxdy=\int xu_0H(\phi)dxdy\\ &a_1\int yH(\phi)dxdy+b_1\int xyH(\phi)dxdy+c_1\int[y^2+\mu]H(\phi)dxdy\\ &=\int yu_0H(\phi)dxdy\end{aligned} \tag{78}$$

Similar to the above, we have

$$\frac{\partial E}{\partial a_2}=0,\frac{\partial E}{\partial b_2}=0,\frac{\partial E}{\partial c_2}=0. \tag{79}$$

Or

$$a_2\int(1-H(\phi))dxdy+b_2\int(1-H(\phi))xdxdy$$

$$
\begin{aligned}
&+c_2\int y(1-H(\phi))dxdy = \int u_0(1-H(\phi))dxdy \\
&a_2\int x(1-H(\phi))dxdy + b_2\int [x^2+\mu](1-H(\phi))dxdy \\
&+c_2\int xy(1-H(\phi))dxdy = \int xu_0(1-H(\phi))dxdy \\
&a_2\int y(1-H(\phi))dxdy + +b_2\int xy(1-H(\phi))dxdy + \\
&c_2\int [y^2+\mu](1-H(\phi))dxdy = \int yu_0(1-H(\phi))dxdy
\end{aligned} \tag{80}
$$

In the following, we will prove that $\frac{\partial E}{\partial t} \leq 0$. That is $E(a_i, b_i, c_i, C)$ will decrease in time. Therefore the final solution of Eq.(76) should minimize the functional $E(a_i, b_i, c_i, C)$.

From Eq.(69), we have

$$
\begin{aligned}
\frac{\partial E(a_i,b_i,c_i,C)}{\partial t} &= \int [(a_1+b_1x+c_1y-u_0)^2\delta(\phi)\frac{\partial \phi}{\partial t} - (a_2+b_2x+c_2y-u_0)^2\delta(\phi)\frac{\partial \phi}{\partial t}]dxdy \\
&+\nu\int \frac{\partial \delta(\phi)}{\partial \phi}\frac{\partial \phi}{\partial t}|\nabla(\phi)|dxdy + \nu\int \delta(\phi)\frac{\partial |\nabla(\phi)|}{\partial \phi_x}\frac{\partial \phi_x}{\partial t}dxdy \\
&+\nu\int \delta(\phi)\frac{\partial |\nabla(\phi)|}{\partial \phi_y}\frac{\partial \phi_y}{\partial t}dxdy
\end{aligned} \tag{81}
$$

Using the fact that

$$
\frac{\partial \phi_y}{\partial t} = \frac{\partial(\frac{\partial \phi}{\partial t})}{\partial y}, \qquad \frac{\partial \phi_x}{\partial t} = \frac{\partial(\frac{\partial \phi}{\partial t})}{\partial x} \tag{82}
$$

Then Eq.(81) becomes:

$$
\begin{aligned}
\frac{\partial E(a_i,b_i,c_i,C)}{\partial t} &= \int [(a_1+b_1x+c_y-u_0)^2\delta(\phi)\frac{\partial \phi}{\partial t} - (a_2+b_2x+c_2y-u_0)^2\delta(\phi)\frac{\partial \phi}{\partial t}]dxdy \\
&+\nu\int \frac{\partial \delta(\phi)}{\partial \phi}\frac{\partial \phi}{\partial t}|\nabla(\phi)|dxdy \\
&+\nu\int \nabla\cdot(\vec{B}\frac{\partial \phi}{\partial t})dxdy - \nu\int (\nabla\cdot\vec{B})\frac{\partial \phi}{\partial t}dxdy
\end{aligned} \tag{83}
$$

with

$$
\vec{B} = \delta(\phi)(\frac{\partial |\nabla\phi|}{\partial \phi_x}, \frac{\partial |\nabla\phi|}{\partial \phi_y}) = \delta(\phi)\frac{\nabla\phi}{|\nabla\phi|}. \tag{84}
$$

Because the boundary condition of the Euler-Lagrange equation

$$\int \nabla \cdot \vec{B} dxdy = \int \vec{B} \cdot \vec{n} dl = 0, \tag{85}$$

and

$$\nabla \cdot \vec{B} = \delta'(\phi)|\nabla\phi| + \delta(\phi)\nabla \cdot \frac{\nabla\phi}{|\nabla\phi|}, \tag{86}$$

we have

$$\begin{aligned} \frac{\partial E(a_i, b_i, c_i, C)}{\partial t} &= -\int \Big\{\delta(\phi)[(a_1 + b_1 x + c_1 y - u_0)^2 + (a_2 + b_2 x + c_2 y - u_0)^2 \\ &\quad -\nu\nabla \cdot (\frac{\nabla\phi}{|\nabla\phi}|)]\Big\}^2 dxdy \\ &= -\int L_{linear}(\phi)^2 dxdy \leq 0. \end{aligned} \tag{87}$$

Thus we have shown in Eq.(87) that $\frac{\partial E}{\partial t} \leq 0$.

3.3 Experimental results of linear approximation for one level set

We have implemented the above model using the method developed in [23]. The segmentation results of three Chinese characters are shown in Fig. 19. It is clear that our method gives good segmentation results. In Fig. 20, the MS energy vs time is shown. The graph shows that the MS energy decreases with time.

In Fig. 21, we show the segmentation results by using the Chan-Vese model and our model. Our model gives a much better segmentation results compared to the Chan-Vese model. Our model can obtain detailed structure inside the image. We have also shown in the figure the energy vs time. It is clear that the MS energy of the linear approximation MS model is smaller than the energy of the piecewise constant MS model.

In Figs. 22 to 24, more examples of segmentation using the piecewise constant and linear approximation MS models are shown. These results show us that this linear approximation model can produce better segmentation results. For example, in Fig. 24, the piecewise constant MS model can not produce a good segmentation for the lower part of the image. However our model can provide better results.

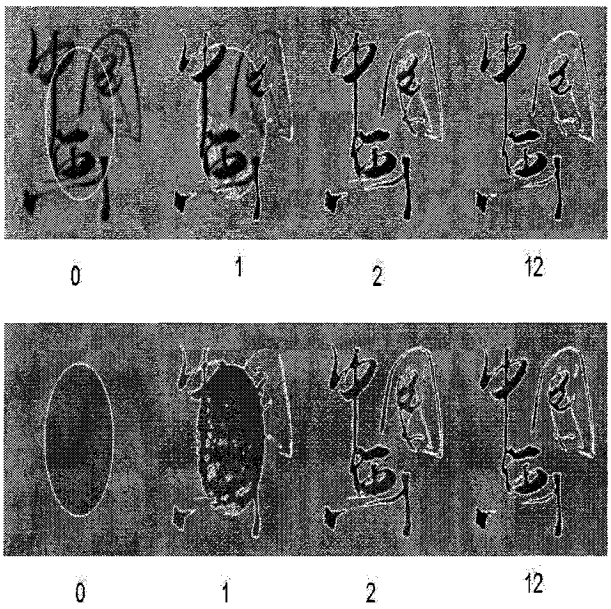

Figure 19: *The images show the evolution of the $\phi(x, y, t)$. In the calculation, we have approximated the two phases by two planes. It is clear after two iterations, we almost get the final segmentation results. In the calculation, we choose $\nu = 0.5\sigma^2$. σ^2 is the variation of the input image.*

3.4 The four-phase linear approximation

To investigate more detailed structure of an image, we need more level sets. For two level set functions ϕ_1, ϕ_2, the four-phase linear approximation Mumford-Shah model can be written as

$$
\begin{aligned}
&E_4^{linear}(a_{ij}, b_{ij}, c_{ij}, \phi_1, \phi_2) = \\
&\int (u_0 - a_{11} - b_{11}x - c_{11}y)^2 H(\phi_1)H(\phi_2)dxdy \\
&+ \int (u_0 - a_{10} - b_{10}x - c_{10}y)^2 H(\phi_1)(1 - H(\phi_2))dxdy \\
&+ \int (u_0 - a_{01} - b_{01}x - -c_{01}y)^2 (1 - H(\phi_1))H(\phi_2)dxdy \\
&+ \int (u_0 - a_{00} - b_{00}x - c_{00}y)^2 (1 - H(\phi_1))(1 - H(\phi_2))dxdy \\
&+\mu(b_{11}^2 + c_{11}^2) \int H(\phi_1)H(\phi_2)dxdy \\
&+\mu(b_{10}^2 + c_{10}^2) \int H(\phi_1)(1 - (H(\phi_2))dxdy \\
&+\mu(b_{01}^2 + c_{01}^2) \int (1 - H(\phi_1))H(\phi_2)dxdy
\end{aligned}
$$

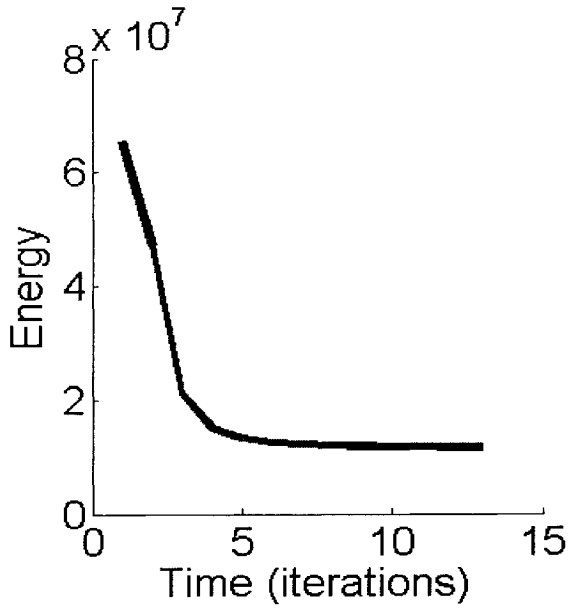

Figure 20: *The MS Energy vs time (iterations) is shown.*

$$+\mu(b_{00}^2+c_{00}^2)\int(1-H(\phi_1))(1-(H(\phi_2))dxdy$$
$$+\nu\int|\nabla H(\phi_1)|dxdy+\nu\int|\nabla H(\phi_2)|dxdy. \tag{88}$$

Let

$$\begin{aligned}
F_4^{linear}(\phi_1,\phi_2) &= (u_0-a_{11}-b_{11}x-c_{11}y)^2H(\phi_1)H(\phi_2)\\
&+(u_0-a_{10}-b_{10}x-c_{10}y)^2H(\phi_1)(1-H(\phi_2))\\
&+(u_0-a_{01}-b_{01}x-c_{01}y)^2(1-H(\phi_1))H(\phi_2)\\
&+(u_0-a_{00}-b_{00}x-c_{00}y)^2(1-H(\phi_1))(1-H(\phi_2))\\
&+\mu(b_{11}^2+c_{11}^2)H(\phi_1)H(\phi_2)+\mu(b_{10}^2+c_{10}^2)H(\phi_1)(1-(H(\phi_2))\\
&+\mu(b_{01}^2+c_{01}^2)(1-H(\phi_1))H(\phi_2)+\mu(b_{00}^2+c_{00}^2)(1-H(\phi_1))(1-(H(\phi_2))\\
&+\nu|\nabla H(\phi_1)|+\nu|\nabla H(\phi_2)|
\end{aligned} \tag{89}$$

we have

$$\begin{aligned}
\frac{\partial F_4^{linear}}{\partial\phi_1} &= (a_{11}+b_{11}x+c_{11}y-u_0)^2\delta(\phi_1)H(\phi_2)\\
&+(a_{10}+b_{10}x+c_{10}y-u_0)^2\delta(\phi_1)(1-H(\phi_2))\\
&-(a_{01}+b_{01}x+c_{01}y-u_0)^2\delta(\phi_1)H(\phi_2)
\end{aligned}$$

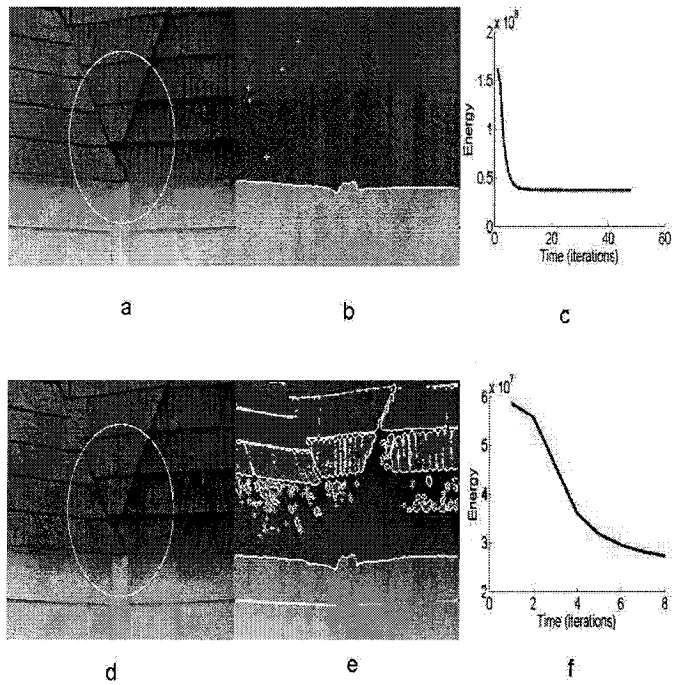

Figure 21: *Segmentation results of a roof edge image. (a): Original image and initial level set for the piecewise constant model, (b): Segmentation result of piecewise constant MS model, (c): energy vs time for the piecewise constant model, (d): Original image and initial level set for the linear approximation model, (e): Segmentation result of the linear approximation MS model, (f): energy vs time for the linear approximation MS model. In the calculation,* $\nu = 0.5\sigma^2$ *and* σ^2 *is the variation of the input image,* $\mu = 0$.

$$
\begin{aligned}
&-(a_{00} + b_{00}x + c_{00}y - u_0)^2\delta(\phi_1)(1 - H(\phi_2)) \\
&+\mu(b_{11}^2 + c_{11}^2)\delta(\phi_1)H(\phi_2) + \mu(b_{10}^2 + c_{10}^2)\delta(\phi_1)(1 - (H(\phi_2)) \\
&-\mu(b_{01}^2 + c_{01}^2)\delta(\phi_1))H(\phi_2) - \mu(b_{00}^2 + c_{00}^2)\delta(\phi_1))(1 - (H(\phi_2)) \\
&+\nu\delta'(\phi_1)|\nabla\phi_1| \qquad (90)
\end{aligned}
$$

and

$$
\nabla \cdot (\frac{\partial}{\partial x}(\frac{\partial F_4}{\partial \phi_{1x}}), \frac{\partial}{\partial y}(\frac{\partial F_4}{\partial \phi_{1y}})) \quad = \quad \nu[\delta'(\phi_1)|\nabla\phi_1| + \delta(\phi_1)\nabla \cdot \frac{\nabla\phi_1}{|\nabla\phi_1|}] \qquad (91)
$$

We have the following Euler-Lagrange equation for ϕ_1:

$$
\begin{aligned}
&\delta(\phi_1)\Big[[(a_{11} + b_{11}x + c_{11}y - u_0)^2 + \mu(b_{11}^2 + c_{11}^2) \\
&-(a_{01} + b_{01}x + c_{01}y - u_0)^2 - \mu(b_{01}^2 + c_{01}^2)]H(\phi_2)+
\end{aligned}
$$

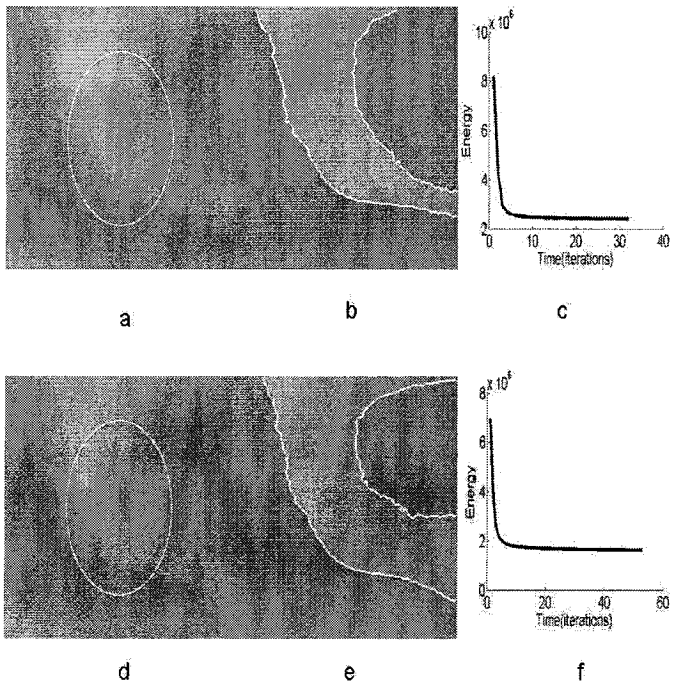

Figure 22: *Segmentation results of an artificial image. (a): Original image and initial level set for the piecewise constant model, (b): Segmentation result of piecewise constant MS model, (c): energy vs time for the piecewise constant model, (d): Original image and initial level set for the linear approximation model, (e): Segmentation result of the linear approximation MS model, (f): energy vs time for the linear approximation MS model. In the calculation,* $\nu = 0.5\sigma^2$ *and* σ^2 *is the variation of the input image,* $\mu = 0$.

$$\begin{aligned}
&[(a_{10} + b_{10}x + c_{10}y - u_0)^2 + \mu(b_{10}^2 + c_{10}^2) \\
&-(a_{00} + b_{00}x + c_{00}y - u_0)^2 - \mu(b_{00}^2 + c_{00}^2)](1 - H(\phi_2)) \\
&-\nu\nabla \cdot (\frac{\nabla\phi_1}{|\nabla\phi_1}) \Big] = 0
\end{aligned} \tag{92}$$

with the boundary condition (see Appendix A)

$$\frac{\delta(\phi_1)}{|\nabla\phi_1|}\nabla\phi_1 \cdot \hat{n} = \frac{\delta(\phi_1)}{|\nabla\phi_1|}\frac{\partial\phi_1}{\partial n} = 0. \tag{93}$$

Here $\hat{n}$ is the normalized normal of the boundary curve of the image.

Similarly, we can derive the Euler-Lagrangian equation for ϕ_2.

$$\frac{\partial F_4}{\partial\phi_2} = (a_{11} + b_{11}x + c_{11}y - u_0)^2\delta(\phi_2)H(\phi_1)$$

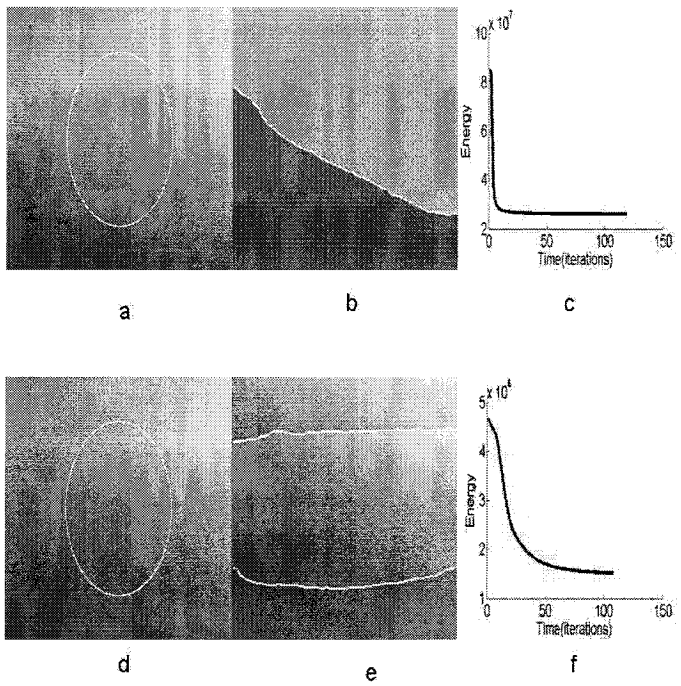

Figure 23: *Segmentation results of an artificial image. (a): Original image and initial level set for the piecewise constant model, (b): Segmentation result of piecewise constant MS model, (c): energy vs time for the piecewise constant model, (d): Original image and initial level set for the linear approximation model, (e): Segmentation result of the linear approximation MS model, (f): energy vs time for the linear approximation model. In the calculation,* $\nu = 0.5\sigma^2$ *and* σ^2 *is the variation of the input image,* $\mu = 0$.

$$
\begin{aligned}
&-(a_{10} + b_{10}x + c_{10}y - u_0)^2 H(\phi_1)\delta(\phi_2) \\
&+(a_{01} + b_{01}x + c_{01}y - u_0)^2 \delta(\phi_2)(1 - H(\phi_1)) \\
&-(a_{00} + b_{00}x + c_{00}y - u_0)^2 (1 - H(\phi_1))\delta(\phi_2) \\
&+\mu(b_{11}^2 + c_{11}^2)\delta(\phi_2)H(\phi_1) - \mu(b_{10}^2 + c_{10}^2)H(\phi_1)\delta(\phi_2) \\
&+\mu(b_{01}^2 + c_{01}^2)\delta(\phi_2)(1 - H(\phi_1)) - \mu(b_{00}^2 + c_{00}^2)^2(1 - H(\phi_1))\delta(\phi_2) \\
&+\nu\delta'(\phi_2)|\nabla\phi_1|
\end{aligned} \tag{94}
$$

and

$$
\nabla \cdot (\frac{\partial}{\partial x}(\frac{\partial F_4}{\partial \phi_{2x}}), \frac{\partial}{\partial y}(\frac{\partial F_4}{\partial \phi_{2y}})) = \nu[\delta'(\phi_2)|\nabla\phi_2| + \delta(\phi_2)\nabla \cdot \frac{\nabla\phi_2}{|\nabla\phi_2|} \tag{95}
$$

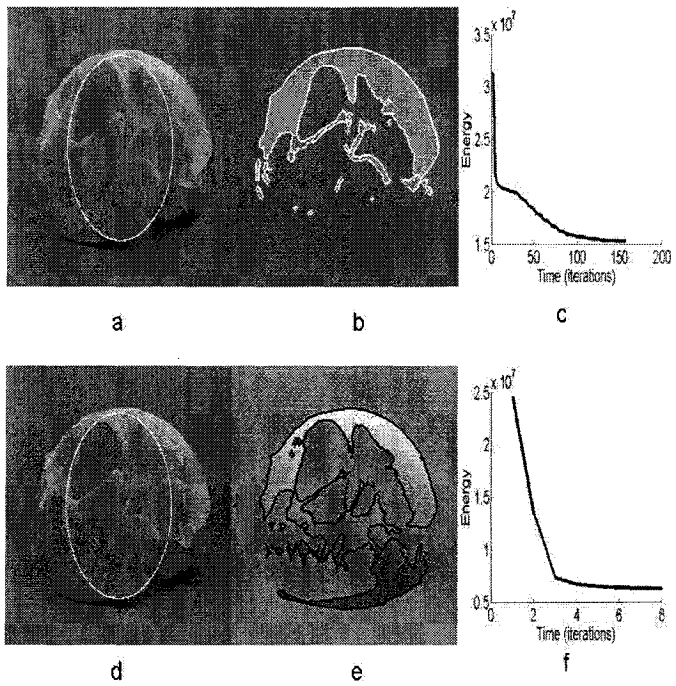

Figure 24: *Segmentation results of a bone image. (a): Original image and initial level set for the piecewise constant model, (b): Segmentation result of piecewise constant MS model, (c): energy vs time for the piecewise constant model, (d): Original image and initial level set for the linear approximation model, (e): Segmentation result of the linear approximation MS model, (f): energy vs time for the linear approximation model. In the calculation,* $\nu = 0.05\sigma^2$ *and* σ^2 *is the variation of the input image,* $\mu = 0$.

Therefore, we have the following Euler-Lagrange equation for ϕ_2:

$$\begin{aligned}
&\delta(\phi_2)\Big[[(a_{11}+b_{11}x+c_{11}y-u_0)^2+\mu(b_{11}^2+c_{11}^2)\\
&-(a_{10}+b_{10}x+c_{10}y-u_0)^2-\mu(b_{10}^2+c_{10}^2)]H(\phi_1)+\\
&[(a_{01}+b_{01}x+c_{01}y-u_0)^2+\mu(b_{01}^2+c_{01}^2)\\
&-(a_{00}+b_{00}x+c_{00}y-u_0)^2-\mu(b_{00}^2+c_{00}^2)](1-H(\phi_1))\\
&-\nu\nabla\cdot(\frac{\nabla\phi_2}{|\nabla\phi_2|})\Big]=0
\end{aligned} \tag{96}$$

with the boundary condition(see Appendix A)

$$\frac{\delta(\phi_2)}{|\nabla\phi_2|}\nabla\phi_2\cdot\hat{n}=\frac{\delta(\phi_2)}{|\nabla\phi_2|}\frac{\partial\phi_2}{\partial n}=0. \tag{97}$$

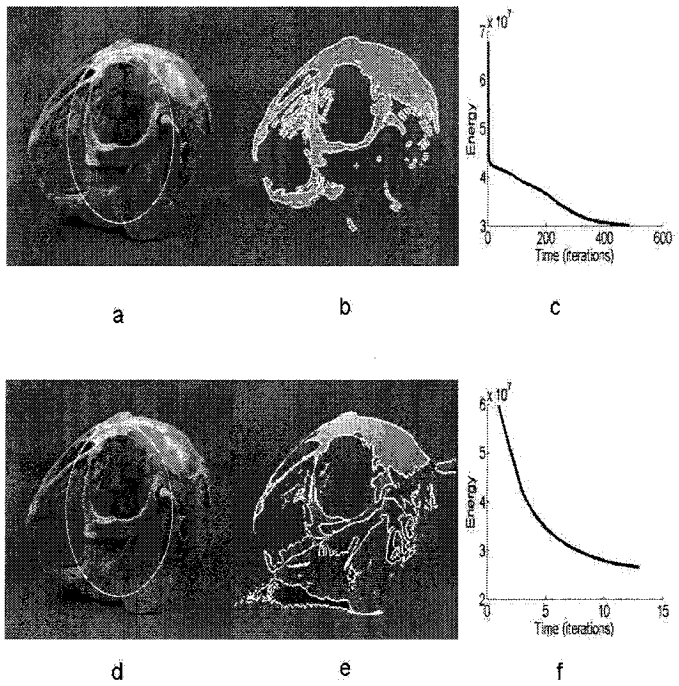

Figure 25: *Segmentation results of a bone image. (a): Original image and initial level set for the piecewise constant model, (b): Segmentation result of piecewise constant MS model, (c): energy vs time for the piecewise constant model, (d): Original image and initial level set for the linear approximation model, (e): Segmentation result of the piecewise constant MS model, (f): energy vs time for the linear approximation model. In the calculation,* $\nu = 0.05\sigma^2$ *and* σ^2 *is the variation of the input image,* $\mu = 0$.

Here $\hat{n}$ is the normalized normal of the boundary curve of the image.

We need to notice that Eq.(92) and Eq.(96) are two coupled equations. We will denote the LHS of Eq.(92) and Eq.(96) by $L_1^{linear}(\phi_1, \phi_2)$ and $L_2^{linear}(\phi_1, \phi_2)$ respectively. Using the gradient projection method, we have the following equations:

$$\frac{\partial \phi_1}{\partial t} = -L_1^{linear} \qquad \frac{\partial \phi_2}{\partial t} = -L_2^{linear} \tag{98}$$

Similarly, we can also prove that $\frac{\partial E_4}{\partial t} \leq 0$. The derivation is similar to the derivation of the two level set case in the Chapter 1 except that we use $a_{ij} + b_{ij}x + c_{ij}y$ to replace c_{ij} in Eq.(52). For the benefit of space, we will neglect the derivation here. We have

$$\frac{\partial E(u, C)}{\partial t} = -\int [(L_1^{linear})^2 + (L_2^{linear})^2] dxdy \leq 0 \tag{99}$$

The shortcoming of two level set methods is that it depends strongly on the initial conditions. Thus we will also use the hierarchical multiphase segmentation method as suggested in [9].

3.5 The hierarchical multiphase segmentation method

For the hierarchical multiphase segmentation method, we will first solve the one level set equation for ϕ_1.

$$\frac{\partial \phi_1}{\partial t} = \delta(\phi_1)[\nu \nabla \cdot \frac{\nabla \phi_1}{|\nabla \phi_1|} - (u_0 - a_1 - b_1 x - c_1 y)^2 - \mu(b_1^2 + c_1^2) \\ +(u_0 - a_2 - b_2 x - c_2 y)^2 + \mu(b_2^2 + c_2^2)] \tag{100}$$

We then obtain two regions defined by $\phi_1 > 0$ and $\phi_1 < 0$.

After the first stage, we use one level set PDE equation for each region separately. That is for region I ($\phi_1 > 0$), we have

$$\frac{\partial \phi_2}{\partial t} = \delta(\phi_2)[\nu_1 \nabla \cdot \frac{\nabla \phi_1}{|\nabla \phi_1|} - (u_0 - a_{11} + b_{11} x - c_{11})^2 - \mu(b_{11}^2 + c_{11}^2) \\ +(u_0 - a_{10} - b_{10} x - c_{10} y)^2 + \mu(b_{10}^2 + c_{10}^2)]. \tag{101}$$

For sub-region II($\phi_1 < 0$), we have

$$\frac{\partial \phi_2}{\partial t} = \delta(\phi_2)[\nu_2 \nabla \cdot \frac{\nabla \phi_1}{|\nabla \phi_1|} - (u_0 - a_{01} - b_{01} x - c_{01} y)^2 - \mu(b_{01}^2 + c_{01}^2) \\ +(u_0 - a_{00} - b_{00} x - c_{00} y)^2 + \mu(b_{00}^2 + c_{00}^2)]. \tag{102}$$

This approach corresponds to solving the one level set equation 3 times. The advantages of this method are that the results do not depend on the initial conditions, and the PDE's are decoupled.

Here we need to point out that Eq.(101) and Eq.(102) come from the second equation of Eq.(98) which is

$$\begin{aligned} \frac{\partial \phi_2}{\partial t} &= -\delta(\phi_2)\Big[[(a_{11} + b_{11} x + c_{11} y - u_0)^2 + \mu(b_{11}^2 + c_{11}^2) \\ &\quad -(a_{10} + b_{10} x + c_{10} y - u_0)^2 - \mu(b_{10}^2 + c_{10}^2)]H(\phi_1) + \\ &\quad [(a_{01} + b_{01} x + c_{01} y - u_0)^2 + \mu(b_{01}^2 + c_{01}^2) - \end{aligned}$$

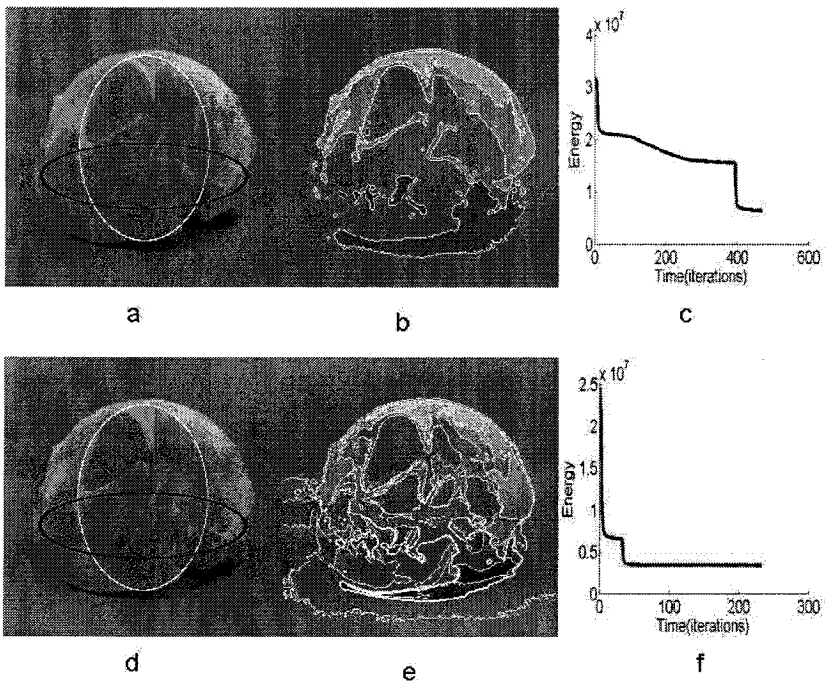

Figure 26: *Segmentation results of two level set method.* (a) : *the original image and initial level sets* (b) : *segmentation result,* (c) : *energy vs time for piecewise constant MS model,* (d) : *the original image and initial level sets* (e) : *segmentation result,* (f) : *the energy vs. time (iterations) for linear approximation MS model. In the calculation,* $\nu = 0.5\sigma^2$ *and* σ^2 *is the variation of the input image,* $\mu = 0$. $\nu_1 = 0.01\sigma_1^2$ *and* $\nu_2 = 0.01\sigma_2^2$. *Here* σ_1^2 *and* σ_2^2 *are variations in region I and region II.*

$$\begin{aligned} &(a_{00} + b_{00}x + c_{00}y - u_0)^2 - \mu(b_{00}^2 + c_{00}^2)](1 - H(\phi_1)) \\ &-\nu\nabla \cdot (\frac{\nabla\phi_2}{|\nabla\phi_2}) \Big] . \end{aligned} \tag{103}$$

If $\phi_1 > 0$, $H(\phi_1) = 1$ and $1 - H(\phi_1) = 0$, thus we get Eq.(101) from Eq.(103). If $\phi_1 < 0$, $H(\phi_1) = 0$ and $1 - H(\phi_1) = 1$, thus we get Eq.(102) from Eq.(103).

3.6 Experimental results of hierarchical multiphase method

In Fig. 26, we show the segmentation results for both piecewise constant and linear approximation MS models. It is clear that the linear approximation is better than the piecewise constant model for this image. The energy vs time is also shown for both models. The final state energy of the linear approximation MS model is smaller

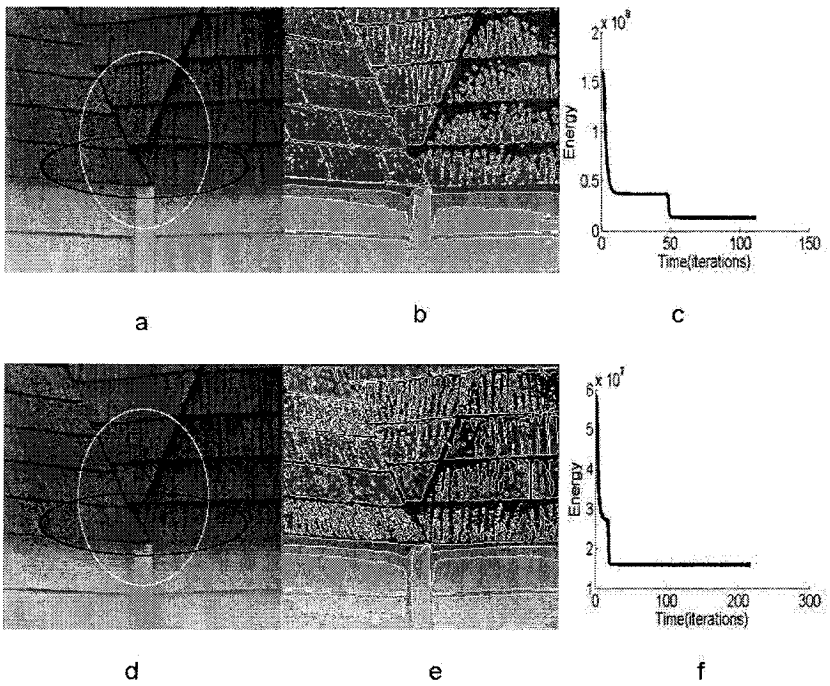

Figure 27: *Segmentation results of two level set method.* (a) : *the original image and initial level sets* (b) : *segmentation result,* (c) : *energy vs time for piecewise constant MS model,* (d) : *the original image and initial level sets* (e) : *segmentation result,* (f) : *the energy vs. time (iterations) for linear approximation MS model. In the calculation,* $\nu = 0.5\sigma^2$ *and* σ^2 *is the variation of the input image,* $\mu = 0$. $\nu_1 = 0.01\sigma_1^2$ *and* $\nu_2 = 0.01\sigma_2^2$. *Here* σ_1^2 *and* σ_2^2 *are variations in region I and region II.*

than that of the piecewise constant MS model.

In Fig. 27, we show another segmentation results of roof edges. It shows in Fig. 21 that one level set linear approximation can give us much better results than the piecewise model. This is because the variation of the intensity in the image is large. For the two level set method, we have shown that linear approximation can also give better segmentation results. It is clear that linear approximation can detect more detailed structure of the image.

3.7 Conclusions and comments

The piecewise constant model can not obtain good segmentation results for images which have large intensity variations inside each region. In this chapter, we have used a linear approximation MS model to model this kind of images and as expected we

have found that this model can produce better segmentation results than the piecewise constant model. We have proved explicitly that the MS energy will decrease vs. time for two phases and four phases approaches.

Of course, in principle, we should solve the original PDE equations for the image function u_0. However this is an ill-posed problem and the calculation time would be impossible for real applications. Therefore, approximation methods used in this chapter and Chapter 1 should be of interest for practical applications.

Chapter 4

The Effects of μ and ν in the Mumford-Shah Model

4.1 Introduction

In Chapter 1, we have mentioned that the MS energy depends on the two parameters μ and ν. It is clear that if μ is very large, the contribution from the second term of Eq.(5) will be significant. To minimize the MS energy, we need to have a small ∇u, that is if $\mu \to \infty$, then ∇u must tend to 0 otherwise the MS energy will approach infinity. Similarly, we can see that if $\nu \to \infty$, then the total length of the level set must approach zero. From this argument, we see that the MS energy depends on the parameters μ and ν. This will be the main topic to investigate in this chapter.

From Eq.(5), we observe that the dimension of $\sqrt{\mu}$ is length and the dimension of $\sqrt{\nu}$ is intensity. In the following we will show that $\sqrt{\mu}$ is a characteristic length or scale of the image and ν is connected with the contrast of the image.

4.2 μ-dependence in the MS model

The two-phase energy function of Eq.(5) can be written as

$$\begin{aligned} E(u_i, C) &= \int_{inside\ C} (u_1 - u_0)^2 dxdy + \int_{outside\ C} (u_2 - u_0)^2 dxdy \\ &\quad + \mu \int_{inside\ C} |\nabla u_1|^2 dxdy + \mu \int_{outside\ C} |\nabla u_2|^2 dxdy + \nu |C| \end{aligned}$$

$$
\begin{aligned}
= & \int (u_1 - u_0)^2 H(\phi) dx\ dy + \int (u_2 - u_0)^2 (1 - H(\phi)) dx dy \\
& + \mu \int |\nabla u_1|^2 H(\phi) dx dy + \mu \int |\nabla u_2|^2 (1 - H(\phi)) dx dy \\
& + \nu \int |\nabla H(\phi)| dx dy. \qquad (104)
\end{aligned}
$$

If we define:

$$
\begin{aligned}
F(\phi) = & (u_1 - u_0)^2 H(\phi) + (u_2 - u_0)^2 (1 - H(\phi)) + \\
& + \mu |\nabla u_1|^2 H(\phi) + \mu |\nabla u_2|^2 (1 - H(\phi)) + \nu \delta(\phi) |\nabla \phi| \qquad (105)
\end{aligned}
$$

and follow the derivation given in Appendix A, we have

$$
\begin{aligned}
\frac{\partial F}{\partial \phi} = & (u_1 - u_0)^2 \delta(\phi) - (u_2 - u_0)^2 \delta(\phi)) + \\
& \mu |\nabla u_1|^2 \delta(\phi) - \mu |\nabla u_2|^2 \delta(\phi) + \nu [\delta'(\phi) |\nabla \phi|] \qquad (106)
\end{aligned}
$$

and

$$
\frac{\partial}{\partial y}(\frac{\partial F}{\partial \phi_x}) = \nu [\delta'(\phi) \frac{\phi_x^2}{\sqrt{\phi_x^2 + \phi_y^2}} + \delta(\phi) \frac{\partial}{\partial x} \frac{\phi_x}{\sqrt{\phi_x^2 + \phi_y^2}}] \qquad (107)
$$

and

$$
\frac{\partial}{\partial y}(\frac{\partial F}{\partial \phi_y}) = \nu [\delta'(\phi) \frac{\phi_y^2}{\sqrt{\phi_x^2 + \phi_y^2}} + \delta(\phi) \frac{\partial}{\partial y} \frac{\phi_y}{\sqrt{\phi_x^2 + \phi_y^2}}] \qquad (108)
$$

Thus, we have the following Euler-Lagrange equation:

$$
\delta(\phi)[(u_1 - u_0)^2 - (u_2 - u_0)^2 + \mu |\nabla u_1|^2 - \mu |\nabla u_2|^2 - \nu \nabla \cdot (\frac{\nabla \phi}{|\nabla \phi}|)] = 0 \qquad (109)
$$

with the boundary condition (see Appendix A)

$$
\frac{\delta(\phi)}{|\nabla \phi|} \nabla \phi \cdot \hat{n} = \frac{\delta(\phi)}{|\nabla \phi|} \frac{\partial \phi}{\partial n} = 0. \qquad (110)
$$

Here $\hat{n}$ is the normalized normal of the boundary curve of the image.

In the following, we will denote the LHS of Eq.(109) by $L(\phi)$. Using the gradient

projection method, we can change Eq.(109) to the following time dependent equation

$$\frac{\partial \phi}{\partial t} = -L(\phi) = \delta(\phi)[-(u_1 - u_0)^2 + (u_2 - u_0)^2 + \nu \nabla \cdot (\frac{\nabla \phi}{|\nabla \phi}|)]. \tag{111}$$

For u_1 and u_2, we can also derive two PDE's

$$\frac{\partial F}{\partial u_1} = 2(u_1 - u_0)H(\phi) \tag{112}$$

and

$$\nabla \cdot (\frac{\partial}{\partial x}(\frac{\partial F}{\partial u_{1x}}), \frac{\partial}{\partial y}(\frac{\partial F}{\partial u_{1y}})) = 2\mu \Delta u_1 H(\phi) \tag{113}$$

Thus the PDE for u_1 is:

$$[(u_1 - u_0) - \mu \Delta u_1]H(\phi) = 0 \tag{114}$$

with boundary condition

$$(u_{1x}, u_{1y}) \cdot \hat{n} = 0. \tag{115}$$

Similarly, the PDE for u_2 is :

$$[(u_2 - u_0) - \mu \Delta u_2](1 - H(\phi)) = 0 \tag{116}$$

with boundary condition

$$(u_{2x}, u_{2y}) \cdot \hat{n} = 0. \tag{117}$$

If $\mu \to \infty$, we have

$$\Delta u_i = 0, \quad i = 1, 2 \tag{118}$$

with the boundary conditions of Eq.(115) and Eq.(117). Therefore, the solution of Eq.(118) are

$$u_i = c_i, \quad i = 1, 2. \tag{119}$$

Where $c_i, i = 1, 2$ are constants. This is consistent with argument in the introduction. That is if $\mu \to \infty$, u_i must be a constant in each region. Therefore the constant approximation is a case corresponding to $\mu \to \infty$.

4.3 μ-dependence of image segmentation

In the following, we will show a simple example to explain the physical meaning of μ. For an one dimension space, the PDE for u can be written as:

$$u - \mu \frac{\partial^2 u}{\partial^2 x} = u_0(x), \tag{120}$$

with boundary condition

$$\frac{\partial u}{\partial x} = 0 \quad x = a, b. \tag{121}$$

Where a, b are the boundary values. If $a = -\infty$ and $b = \infty$, we have

$$u(x) = \int \frac{1}{2\sqrt{\mu}} \exp(-\frac{|x-y|}{\sqrt{\mu}}) u_0(y) dy. \tag{122}$$

From Eq.(122), it is clear that μ is the characteristic size of the image. If $\mu \to 0$, then $u(x) \to u_0$. On the other hand, if $\mu \to \infty$, then $u \to const.$ In other words, if $\mu = 0$, we get almost all information in u_0. On the other hand, if $\mu = \infty$, we lost almost all detail information of the original image. From Eqs.(79),(81), we can see clearly that if $\mu \to \infty$, then $b_1 = c_1 = b_2 = c_2 = 0$.

In Fig. 28, the μ dependence of the segmentation results can be seen for each row. It is clear that if μ-value is very small, the segmentation result contains more detailed information of the original image. The energy vs. time is also shown in Fig. 28. It is clear that the segmentation energy for the case $\mu = 0$ is the smallest among the three cases.

4.4 ν-dependence in the piecewise constant MS model

From Eq.(15), we observe that for a fixed boundary, if ν is very large, then the length term will contribute largely to the total energy $E(u, C)$. On the other hand, if ν is very small, then the length term will contribute very little to the total energy. Since the Chan-Vese model tries to the find the minimal energy of $E(u, C)$. Therefore, if ν is very large, we can not expect very long total boundaries; otherwise it will make

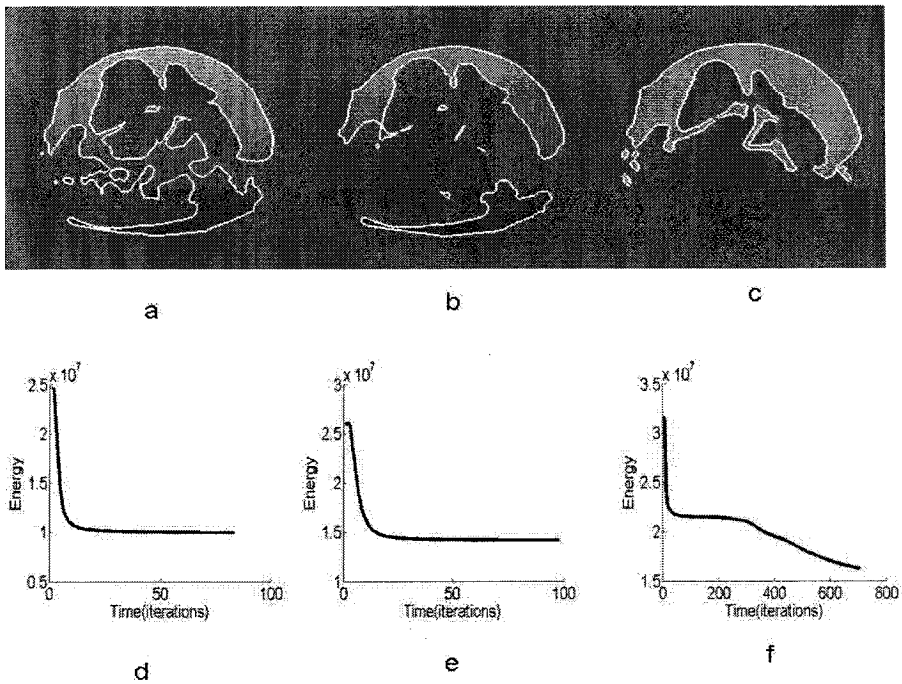

Figure 28: *The segmentation results for different μ. From left to right: $\mu = 0, 1000, \infty$. The corresponding energy vs time is also shown in the second row. Here $\mu = \infty$ refers to piecewise constant case. In the calculation we fix $\nu = \sigma^2$ and σ^2 is the variance of input image.*

$E(u, C)$ large. On the other hand, if ν is very small, then we could find long total boundaries. Because of this, if we try to get the right boundary of some large objects, we have to choose a very small ν. It has been observed in Gao and Bui's paper [9] that when ν becomes very large, the segmentation result of the Chan-Vese model is bad.

In Fig. 29, we show an one dimensional distribution. For this distribution, we can fit by using two constant functions $u(x) = h_1$ for $0 < x < b$ and $u(x) = h_2$ for $-a < x < 0$. Then its MS energy is

$$E_{fit1} = \nu. \tag{123}$$

We can also fit this distribution using a continuous function $u(x)$. It is clear that this $u(x)$ should satisfy the following equation:

$$u - \mu \frac{\partial^2 u}{\partial x^2} = h_1, \tag{124}$$

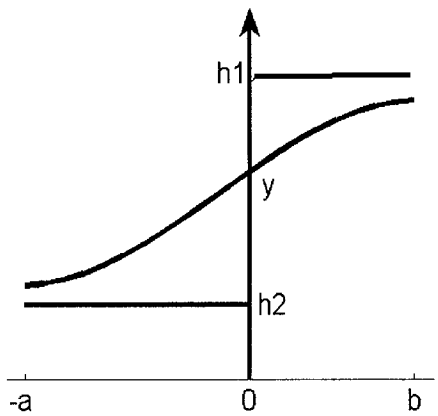

Figure 29: *Two lines with height h_1 and h_2 respectively. The length of the two lines are from $-a$ to 0 and from 0 to b respectively.*

and

$$u - \mu \frac{\partial^2 u}{\partial x^2} = h_2, \tag{125}$$

with the following boundary conditions

$$\frac{\partial u(x)}{\partial x}_{x=-a,b} = 0. \tag{126}$$

and

$$u(x)|_{x=0^+} = u(x)|_{x=0^-}. \tag{127}$$

The above equation actually consists of the following two equations:

$$u - \mu \frac{\partial^2 u}{\partial x^2} = h_1, \tag{128}$$

with boundary conditions

$$\frac{\partial u(x)}{\partial x}_{x=b} = 0, \quad u(x)|_{x=0^+} = y. \tag{129}$$

and

$$u - \mu \frac{\partial^2 u}{\partial x^2} = h_2, \tag{130}$$

with boundary conditions

$$\frac{\partial u(x)}{\partial x}_{x=-a} = 0, \quad u(x)|_{x=0^-} = y. \tag{131}$$

Suppose $w(x)$ is the solution of

$$w - \mu \frac{\partial^2 w}{\partial x^2} = 0 \tag{132}$$

with the boundary condition

$$w(x)|_{x=0} = 1, \quad \frac{\partial w}{\partial x}|_{x=b} = 0. \tag{133}$$

We can explicitly write out the solution of $w(x)$ as

$$w(x) = \frac{cosh(\frac{1}{\sqrt{\mu}}(x-b))}{cosh(\frac{1}{\sqrt{\mu}}b)} \tag{134}$$

The solution of Eq.(128) can be written as

$$u = (y - h_1)w + h_1. \tag{135}$$

Then its MS energy is

$$E_1 = \int_0^b (y-h_1)^2[w^2 + \mu(\frac{\partial w}{\partial x})^2]dx = (y-h_1)^2\sqrt{\mu}\tanh(\frac{b}{\sqrt{\mu}}). \tag{136}$$

Similarly, the solution of Eq.(130) can be written as

$$u = (y - h_2)w + h_2. \tag{137}$$

and its MS energy is

$$E_2 = (y-h_2)^2\sqrt{\mu}\tanh(\frac{a}{\sqrt{\mu}}). \tag{138}$$

Therefore the total MS energy is

$$E_{fit2} = E_1 + E_2 = (y-h_2)^2\sqrt{\mu}\tanh(\frac{a}{\sqrt{\mu}}) + (y-h_1)^2\sqrt{\mu}\tanh(\frac{b}{\sqrt{\mu}}). \tag{139}$$

The energy E depends on the value y and its minimal value satisfies

$$\frac{\partial E}{\partial y} = 0. \tag{140}$$

From Eq.(140), we obtain

$$y = \frac{\sqrt{\mu}tanh(\frac{a}{\sqrt{\mu}})h_2 + \sqrt{\mu}\tanh(\frac{b}{\sqrt{\mu}})h_1}{\sqrt{\mu}\tanh(\frac{b}{\sqrt{\mu}}) + \sqrt{\mu}\tanh(\frac{a}{\sqrt{\mu}})} \tag{141}$$

Thus the minimal MS energy E is

$$E_{fit2} = (h_1 - h_2)^2(\frac{1}{\sqrt{\mu}\tanh(\frac{a}{\sqrt{\mu}})} + \frac{1}{\sqrt{\mu}\tanh(\frac{b}{\sqrt{\mu}})})^{-1}. \tag{142}$$

Suppose $a, b >> \sqrt{\mu}$, we have

$$E_{fit2} = \frac{1}{2}\sqrt{\mu}(h_1 - h_2)^2. \tag{143}$$

So in order to detect this step edge, we must require that $E_{fit1} < E_{fit2}$ or

$$\nu < \frac{1}{2}\sqrt{\mu}(h_1 - h_2)^2 => h_1 - h_2 > h_0 = \sqrt{\frac{2\nu}{\sqrt{\mu}}}. \tag{144}$$

In Eq.(144),we have shown that ν must be small enough for a fixed μ to detect the step edge. In other words, for a fixed ν, only the difference larger than h_0 can be detected.

4.5 A constraint on ν in the piecewise constant model

In Fig. 30, the segmentation results for the piecewise constant MS model are shown for different ν values. It is clear that as ν becomes small, the segmentation results are good. This is due to the fact that when ν becomes small, we could find the small regions which could not be recognized when ν is large. However when ν is very small, regions could not detected due to noise.

In the following, we will show that the value of ν should not be too large and

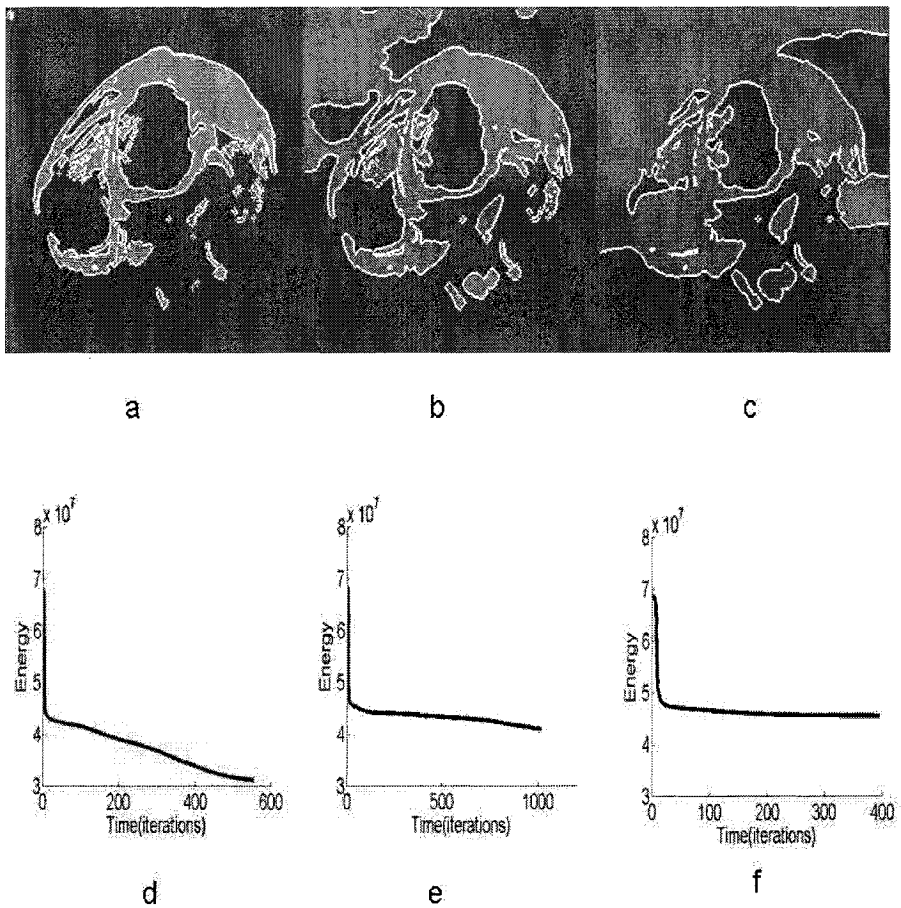

Figure 30: *From left to right:* $\nu = 0.1\sigma^2, 0.5\sigma^2, 1.0\sigma^2$. *Here* σ^2 *is the variance of the input image. The first row is the results of Chan-Vese model and the second row the corresponding energy vs time. The original image is in Fig.16.*

its value is smaller than the variance of the image. Suppose the boundary is empty, $|C| = 0$, then the total energy of the Chan-Vese model of the image is

$$E(u, C) = \int (c - u_0)^2 dxdy = N\sigma^2. \tag{145}$$

Here σ^2 is defined as

$$\sigma^2 = \frac{1}{N}\sum_{i=1}^{N}(u_0(i) - c)^2, c = \frac{1}{N}\sum_{i=1}^{N} u_0(i). \tag{146}$$

N is the total number of pixels on the image and $u_0(i)$ is the pixel value for pixel i.

c is the average pixel value for the image. The Chan-Vese model energy is

$$E(u, C) = \int [(c_1 - u_0)^2 H(\phi) + (c_2 - u_0)^2 (1 - H(\phi)) + \nu |\nabla H(\phi)|] dxdy. \quad (147)$$

According to the Chan-Vese model, the energy in Eq.(147) is smaller than the energy in Eq.(145). Since the last two terms in Eq.(147) are greater than zero, we have

$$\nu |C| \leq N\sigma^2. \quad (148)$$

Since the total length of $|C|$ is proportional to the total number of pixels N and its maximum value is $\sim N$. Thus

$$\nu \leq \sigma^2. \quad (149)$$

Eq.(149) means that we should select ν-value less than the variance of the input image and it is helpful for segmentation experiment.

4.6 More experimental results

In this section more experimental results are shown in Fig. 31. It is clear that as μ becomes large, the detailed information inside the image is lost in the segmentation image. On the other hand, when ν becomes small, some detailed information of the image can be obtained.

4.7 Conclusions and comments

In this chapter, the μ and ν dependences of MS model have been studied. It has been found that when μ is small, detailed information inside each image can be observed. On the other hand, if $\mu \to \infty$, detailed information of the image is lost. Therefore for images that have very large variations, piecewise constant approximation MS model can not provide good segmentation results. When ν is smaller, we can also get detailed structure of the input image. It has been proved that the value of ν should be smaller than the variance of the input image.

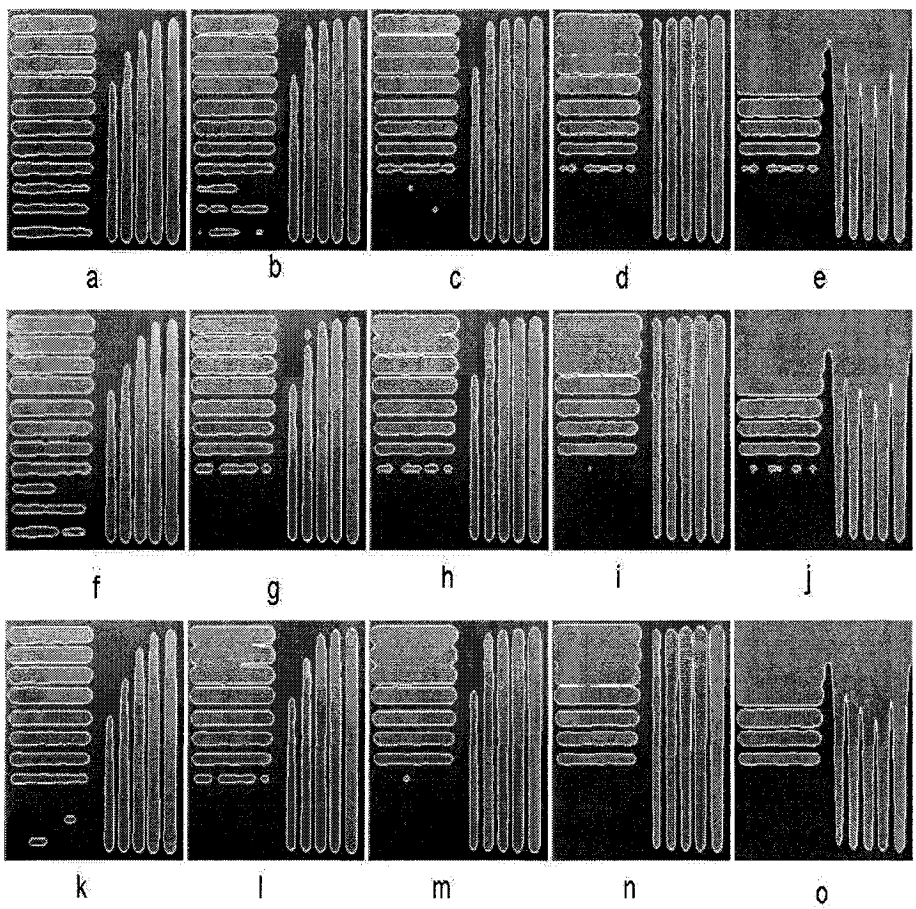

Figure 31: *From left to right:* $\mu = 0, 500, 1000, 3000, \infty$. *From top to bottom:* $\nu = 0.01\sigma^2, 0.5\sigma^2, 1.0\sigma^2$. σ^2 *is the variance of the input image*

Chapter 5

Roof Edge Detection Models

5.1 Introduction

To find the boundary of objects of interest, many methods have been suggested. For example, Sobel and Laplace edge detectors have been used successfully to detect sharp edges of images. However Sobel [48, 49, 50] and Laplace methods calculate the gradient and the second order derivative for each pixel of the observed image. Therefore, only the property of the neighboring pixels is used. These are local approaches. The global property of the input image is neglected in the these methods. On the other hand, the MS model is a global model which involves all the pixels of image in the calculation. To avoid the problem of solving several PDE equations, we have used piecewise constant approximation and linear approximation in the second and third chapters. However, these models can not detect edges that have low contrast.

To deal with edges with low contrast, the MS model can be generalized to the following function form:

$$E(u, C) = \int |u - u_0|^p dxdy + \mu \int_{\Omega C} f(\nabla u) dxdy + \nu \int_C g(|\nabla u|) dl, \tag{150}$$

where $p \geq 1$ and $f(x)$ is a convex function satisfying

$$\lim_{|x| \to \infty} \frac{f(x)}{|x|} = +\infty, \tag{151}$$

and g is an increasing function satisfying

$$\lim_{t\to 0}\frac{g(t)}{t}=\infty. \tag{152}$$

Here we would like to point out that the convex requirement of $f(x)$ is not important since we know that $E(u,C)$ is a non-convex function with length term.

There are many variations of the Mumford-Shah model such as Rudin-Osher-Fatemi (ROF) [36] like model which can be expressed as the following minimization problem:

$$inf_{u,C}\{E_{ROF}(u,C) = \int_{\Omega\setminus C}(u-u_0)^2dxdy+\mu\int_{\Omega\setminus C}|\nabla u|dxdy+\nu|C|\}, \tag{153}$$

The difference between the MS and the ROF like models comes from the second term. In the MS model, the L^p norm with $p=2$ of the gradient allows us to remove the noise but unfortunately penalizes too much the gradient corresponding to edges. One could then decrease p in order to preserve the edges as much as possible. One of the first work in this direction is the ROF model [36].

In this Chapter, we will study some variations of the MS model [43, 45]. Some of the segmentation results are also shown.

5.2 Piecewise constant approximation

If we assume that u is a constant in each region ($u=c$), Eq.(5) and Eq.(153) are of the same form, that is

$$inf_{u,C}\{E(u,C) = \int_{\Omega\setminus C}(c-u_0)^2dxdy+\nu|C|\}. \tag{154}$$

The two-phase version of Eq.(12) can be written as [23, 21, 25, 8, 9]

$$\begin{aligned} E(c_1,c_2,\phi) &= \int_{inside\ C}(c_1-u_0)^2dxdy+\int_{outside\ C}(c_2-u_0)^2dxdy+\nu|C| \\ &= \int_\Omega(c_1-u_0)^2H(\phi)dxdy+\int_\Omega(c_2-u_0^2)(1-H(\phi))dxdy \\ &\quad +\nu\int_\Omega|\nabla H(\phi)|dxdy \end{aligned} \tag{155}$$

where c_1 and c_2 are constants.

We have the following level set equation:

$$\frac{\partial \phi}{\partial t} = -\delta(\phi)[(c_1 - u_0)^2 - (c_2 - u_0)^2 - \nu \nabla \cdot (\frac{\nabla \phi}{|\nabla \phi}|)] \tag{156}$$

with the boundary condition $\frac{\delta(\phi)}{|\nabla \phi|} \nabla \phi \cdot \hat{n} = \frac{\delta(\phi)}{|\nabla \phi|} \frac{\partial \phi}{\partial n} = 0$. The final solution of Eq.(156) will minimize the function $E(c_1, c_2, \phi)$. Because c_1 and c_2 are constants, we have $\frac{\partial E}{\partial c_1} = \frac{\partial E}{\partial c_2} = 0$. Therefore, $c_1(\phi) = \frac{\int_\Omega u_0 H(\phi) dxdy}{\int_\Omega H(\phi) dxdy}$ and $c_2(\phi) = \frac{\int_\Omega u_0 (1 - H(\phi)) dxdy}{\int_\Omega (1 - H(\phi)) dxdy}$.

5.3 ROF model with gradient term

For the piecewise constant approximation, the second term of Eqs. (5) and (153) does not appear and the MS and ROF models are the same. In this case, the whole image is segmented into different regions such that the variance inside each region is small. Therefore the low contrast edges in a region will not be detected since it will not cause much changes to the variance inside that region. In order to detect these small differences, we need to include the gradient term in Eq.(153) in our calculation. To include the gradient in the calculation means that we need to solve two PDEs [1, 7, 15, 19]: one for u inside and one for u outside the curve C. To simplify the problem we use the fact that the final solution of u should be approximately u_0, and we replace the second term of Eq.(153) by $\int |\nabla u_0| dxdy$. Thus, the ROF model becomes:

$$\begin{aligned} inf_{u,C}\{E(u, C) &= \int_{inside\ C} (c_1 - u_0)^2 dxdy + \int_{outside\ C} (c_2 - u_0)^2 dxdy \\ &+ \mu \int_{inside\ C} |\nabla u_0| dxdy + \nu |C|\}, \end{aligned} \tag{157}$$

Notice that for the gradient term, we only calculate the gradient inside C. The advantage of this approximation compared to the original ROF model is that the calculation is fast since we do not need to solve two coupled PDEs for u inside and outside respectively. Therefore, it would be more useful for practical applications. The advantage of this approximation over the piecewise constant case is that more edges can be detected.

The level set equation becomes:

$$\frac{\partial \phi}{\partial t} = -\delta(\phi)[(c_1 - u_0)^2 - (c_2 - u_0)^2 + \mu|\nabla u_0| - \nu\nabla \cdot (\frac{\nabla \phi}{|\nabla \phi}|)], \tag{158}$$

with the boundary condition $\frac{\delta(\phi)}{|\nabla \phi|}\nabla \phi \cdot \hat{n} = 0$. It is clear that when $\mu \to 0$, Eq.(157) becomes Eq.(155).

5.4 ROF model with high order derivative

In both the MS and the ROF original models, high order derivatives of u are not included. We of course can include high order derivative term of u in the models. For example, if we include second derivative of u in ROF, then the ROF model becomes:

$$\begin{aligned} inf_{u,C}\{E(u,C) &= \int_{\Omega \setminus C}(u - u_0)^2 dxdy + \mu \int_{\Omega \setminus C} |\nabla u| dxdy + \\ &+ \lambda \int_{\Omega \setminus C} |\Delta u| dxdy + \int \nu |C|\}, \end{aligned} \tag{159}$$

In order to study only the Laplacian term effects on the segmentation, we will take $\mu = 0$ in Eq.(159). Using $u = u_0$ approximation in the third term of Eq.(159), the above equation for two phases becomes:

$$\begin{aligned} inf_{u,C}\{E(u,C) &= \int_{inside\ C}(c_1 - u_0)^2 dxdy + \int_{inside\ C}(c_2 - u_0)^2 dxdy \\ &+ \lambda \int_{inside\ C} |\Delta u_0| dxdy + \int \nu |C|\}, \end{aligned} \tag{160}$$

In the above, we have only included the Laplacian term for the inside region. Thus, the level set equation changes to

$$\frac{\partial \phi}{\partial t} = -\delta(\phi)[(c_1 - u_0)^2 - (c_2 - u_0)^2 + \lambda|\Delta u_0| - \nu\nabla \cdot (\frac{\nabla \phi}{|\nabla \phi}|)] \tag{161}$$

with the boundary condition $\frac{\delta(\phi)}{|\nabla \phi|}\nabla \phi \cdot \hat{n} = 0$

In [11], Lee, Ben Hamza and Krim have also included the Laplacian term in their analysis. Where they have constructed an energy function as

$$inf_{u,C}\{E(u,C) = \int_{inside\ C}(c_1 - u_0)^2 dxdy + \int_{inside\ C}(c_2 - u_0)^2 dxdy$$

$$+ \int \nu|C| + \beta A - \gamma[\int_{inside\ C} |\Delta u_0| dxdy - \int_{outside\ C} |\Delta u_0| dxdy]\}, \quad (162)$$

Here A is the area inside the curve. Due to the fact that $\int |\Delta u_0| dxdy$ is a constant for a given image. Therefore, the maximum value of $\int_{outside\ C} |\Delta u_0| dxdy - \int_{inside\ C} |\Delta u_0| dxdy$ is the same as the minimum value of $\int_{inside\ C} |\Delta u_0| dxdy$. Therefore the model in Ref. [11] is similar to the above model. If $\lambda = 0$, Eq.(160) becomes to Eq.(155).

5.5 Linear approximation of ROF model

In the MS model, the second term in Eq.(5) leads u to be smooth in each region. However $|\nabla u|$ becomes very large across the boundary line. Therefore the MS model can be used to detect discontinuities in the image surface. They can also be detected by the Chan-Vese (CV) model due to the fact that the variation of the image intensity across the regions becomes very large if the boundaries are step edges. But if the step edge is small, then this kind of boundary will be hard to detect.

In the following, we will use linear approximation instead of constant approximation. We will use a linear planar surface, $u(x, y) = a + b \cdot x + c \cdot y$, to approximate the inside of each region in this section. Here a, b, c are constants. From here onward $\int$ means $\int_\Omega$; for simplicity Ω is omitted.

For the two-phase case, Eq.(153) becomes:

$$\begin{aligned} E_{ROF}(u_1, u_2, \phi) &= \int (a_1 + b_1 x + c_1 y - u_0)^2 H(\phi) dxdy \\ &+ \int (a_2 + b_2 x + c_2 y - u_0)^2 (1 - H(\phi)) dxdy \\ &+ \mu\sqrt{(b_1^2 + c_1^2)} \int H(\phi) dxdy + \mu\sqrt{(b_2^2 + c_2^2)} \int (1 - H(\phi)) dxdy + \\ &\nu \int |\nabla H(\phi)| dxdy. \end{aligned} \quad (163)$$

We obtain the following level-set equation for Eq.(163):

$$\begin{aligned} \frac{\partial \phi}{\partial t} &= -\delta(\phi)[-\nu \nabla \cdot \frac{\nabla \phi}{|\nabla \phi|} + (a_1 + b_1 x + c_1 y - u_0)^2 + \mu\sqrt{(b_1^2 + c_1^2)} \\ &-(a_2 + b_2 x + c_2 y - u_0)^2 - \mu\sqrt{(b_2^2 + c_2^2)}] \end{aligned} \quad (164)$$

with the same boundary condition as Eq.(156).

We can calculate a_1, b_1, c_1 for ROF model via the following equation

$$\begin{aligned}
&a_1 \int H(\phi)dxdy + b_1 \int H(\phi)xdxdy + c_1 \int yH(\phi)dxdy = \int u_0 H(\phi)dxdy \\
&a_1 \int xH(\phi)dxdy + b_1 \int (x^2)H(\phi)dxdy + \frac{\mu b_1}{2\sqrt{b_1^2 + c_1^2}} \int H(\phi)dxdy \\
&+c_1 \int xyH(\phi)dxdy = \int xu_0 H(\phi)dxdy \qquad (165) \\
&a_1 \int yH(\phi)dxdy + +b_1 \int xyH(\phi)dxdy + c_1 \int (y^2)H(\phi)dxdy \\
&+\frac{\mu c_1}{2\sqrt{b_1^2 + c_1^2}} \int H(\phi)dxdy = \int yu_0 H(\phi)dxdy
\end{aligned}$$

We have similar equation for a_2, b_2, c_2 but with $1 - H(\phi)$ replacing $H(\phi)$.

5.6 Experimental results of the ROF model

In Fig. 32, the segmentation results of all the above models are shown. It is clear that the CV constant model cannot detect all the boundaries in the image. On the other hand, all other models give better segmentation results. This is not surprising at all. Since it is well known that the gradient and Laplacian terms can detect the boundary very well for sharp edges. Therefore including the gradient and Laplacian terms in the CV model can give us better results. For linear approximation model of the MS and ROF models, we can expect some detailed information inside each region Ω_i.

In Fig. 33, we have also used the Chan-Vese piecewise constant approximation model, ROF like model with the gradient and Laplacian terms, and the MS and ROF models with linear approximation for the car plate image. It is found that Chan-Vese piecewise constant approximation cannot detect the number 8 in the image while it is detected by other models.

In Fig. 34, we have also used the above models for the bone image. It is found that the ROF like model with the gradient and Laplacian terms, the MS and ROF models with linear approximation gives better results than the piece-wise constant MS model.

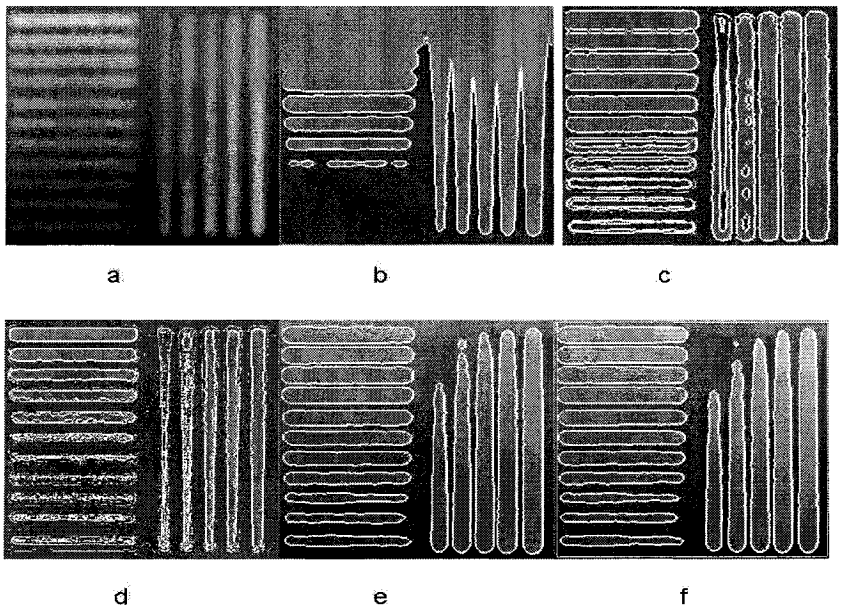

Figure 32: *First row: (a) original image, (b) Chan-Vese piecewise constant approximation. (c) ROF model with the gradient term. Second row: (d) ROF model with Laplacian term, (e) MS model with linear approximation, (f) ROF like model with linear approximation.*

5.7 More on the generalized MS model

In the Mumford-Shah model, the second term in Eq.(5) leads u to be smooth in each region. $|\nabla u|$ will become very large across the boundary line. Therefore the Mumford-Shah model can be used to detect discontinuities in the image surface. This kind of discontinues in image surface is called **step edges**. However there is also a case that the image is continuous but its first order derivative is discontinuous; that is there is a step edge in the first order derivative functional space. This kind of discontinuities is called **roof edges**.

In the MS model, u is required to be smooth in each region. For images that have intensity changes almost everywhere, it is hard to use the MS model to detect the right boundary. In order to detect boundary of this kind of image, we will introduce another generalization of the MS model (Eq.(5)):

$$E_{GMS} = \int_{\Omega\setminus C}(u-u_0)^2 dxdy + \mu \int_{\Omega\setminus C}(\nabla u - \nabla u_0)^2 dxdy + \nu|C|. \tag{166}$$

The difference between Eq.(5) and Eq.(166) comes from the second term. In this new

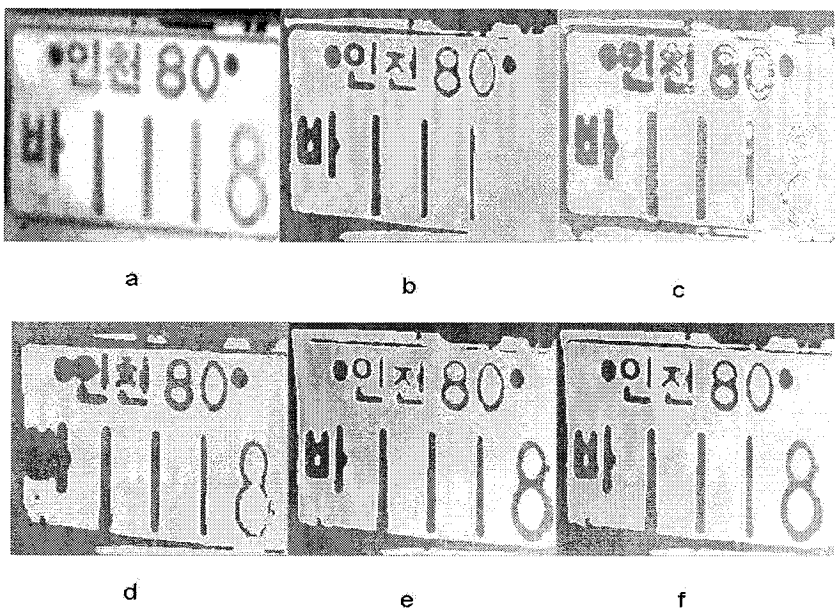

Figure 33: *First row: (a) original image, (b) Chan-Vese piecewise constant approximation. (c) ROF model with the gradient term. Second row: (d) ROF model with Laplacian term, (e) MS model with linear approximation, (f) ROF like model with linear approximation.*

model, we constrain that the gradient of u approaches the gradient of u_0. Unlike Eq.(5), where we constrain that u approaches u_0; here we would like both u and ∇u to approach u_0 and ∇u_0 respectively. Therefore u should be a better approximation to the original image. In the following, we will call Eq.(166) as the generalized Mumford-Shah (GMS) model.

It is clear that if we let $\mu = 0$, then Eq.(166) and Eq.(154) are the same. It is clear that if $\mu \to \infty$ in Eq.(166), we have $\nabla u \to \nabla u_0$. Thus all the variations of the original image u_0 are conserved. However if $\mu \to \infty$ in Eq.(154), we have $\nabla u \to 0$. Thus all the variations of the original image are lost. This short analysis tells us that Eq.(166) is better than Eq.(154) for images which have large variations.

5.7.1 Constant approximation

For the constant approximation $u = c$, the two-phase GMS model can be written as

$$\begin{aligned} E_{GMS}(c_1, c_2, C) &= \int (c_1 - u_0)^2 H(\phi) dxdy + \int (c_2 - u_0)^2 (1 - H(\phi)) dxdy \\ &\quad + \mu \int |\nabla u_0|^2 dxdy + \int \nu |C| \}, \end{aligned} \tag{167}$$

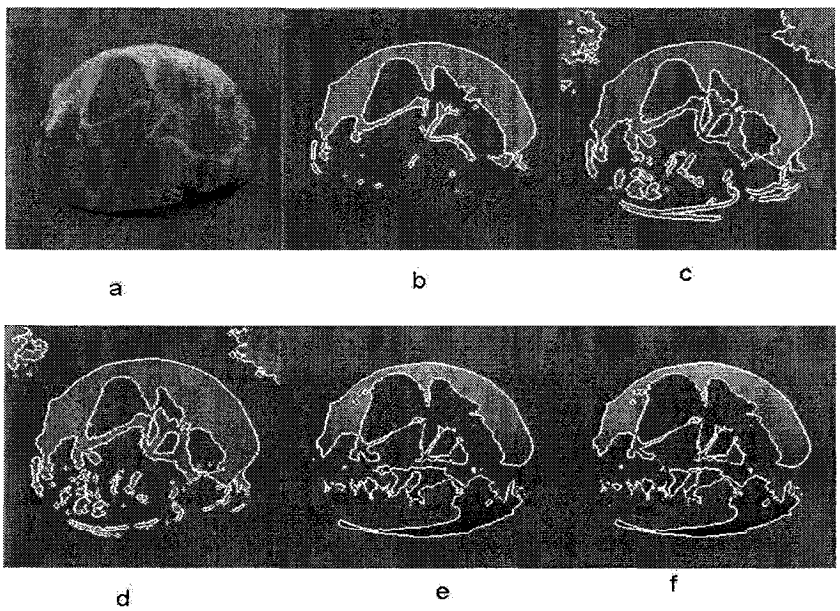

Figure 34: *First row: (a) original image, (b) Chan-Vese piecewise constant approximation. (c) ROF model with the gradient term. Second row: (d) ROF model with Laplacian term, (e) MS model with linear approximation, (f) ROF like model with linear approximation.*

The third term in Eq.(167) is a constant for each input image. So we will change it to:

$$\begin{aligned} E_{GMS}(c_1, c_2, C) &= \int (c_1 - u_0)^2 H(\phi) dxdy + \int (c_2 - u_0)^2 (1 - H(\phi)) dxdy \\ &\quad + \mu \int |\nabla u_0|^2 H(\phi) dxdy + \int \nu |C|\}, \end{aligned} \tag{168}$$

Thus, the level set equation for Eq.(168) is

$$\frac{\partial \phi}{\partial t} = -\delta(\phi)[(c_1 - u_0)^2 - (c_2 - u_0)^2 + \mu(\nabla u_0)^2 - \nu \nabla \cdot (\frac{\nabla \phi}{|\nabla \phi}|)]. \tag{169}$$

This equation is similar to Eq.(158).

5.7.2 Linear approximation

The two-phase linear approximation of the GMS model can be written as

$$E_{GMS}(a_i, b_i, c_i, C) = \int (a_1 + b_1 x + c_1 y - u_0)^2 H(\phi) dxdy$$

$$
\begin{aligned}
&+\int (a_2+b_2x+c_2y-u_0)^2(1-H(\phi))dxdy \\
&+\mu\int[(b_1-\frac{\partial u_0}{\partial x})^2+(c_1-\frac{\partial u_0}{\partial y})^2]H(\phi)dxdy \\
&+\mu\int[(b_2-\frac{\partial u_0}{\partial x})^2+(c_2-\frac{\partial u_0}{\partial y})^2](1-H(\phi))dxdy+ \\
&\int \nu|\nabla H(\phi)|dxdy. \qquad (170)
\end{aligned}
$$

The level set equations for Eq.(170) is

$$
\begin{aligned}
\frac{\partial\phi}{\partial t} &= \delta(\phi)[\nu\nabla\cdot\frac{\nabla\phi}{|\nabla\phi|}-(a_1+b_1x+c_1y-u_0)^2- \\
&\mu[(b_1-\frac{\partial u_0}{\partial x})^2+(c_1-\frac{\partial u_0}{\partial y})^2] \\
&+(a_2+b_2x+c_2y-u_0)^2+ \\
&+\mu[(b_2-\frac{\partial u_0}{\partial x})^2+(c_2-\frac{\partial u_0}{\partial y})^2]] \qquad (171)
\end{aligned}
$$

We can calculate a_1, b_1, c_1 by the following equations

$$
\frac{\partial E}{\partial a_1}=0, \frac{\partial E}{\partial b_1}=0, \frac{\partial E}{\partial c_1}=0. \qquad (172)
$$

Or

$$
\begin{aligned}
&a_1\int H(\phi)dxdy+b_1\int H(\phi)xdxdy \\
&+c_1\int yH(\phi)dxdy=\int u_0H(\phi)dxdy \\
&a_1\int xH(\phi)dxdy+b_1\int(x^2+\mu)H(\phi)dxdy \\
&+c_1\int xyH(\phi)dxdy=\int(xu_0+\mu\frac{\partial u_0}{\partial x})H(\phi)dxdy \qquad (173) \\
&a_1\int yH(\phi)dxdy+b_1\int xyH(\phi)dxdy+c_1\int(y^2+\mu)H(\phi)dxdy \\
&=\int(yu_0+\mu\frac{\partial u_0}{\partial y})H(\phi)dxdy
\end{aligned}
$$

Similar to the above, we have

$$
\frac{\partial E}{\partial a_2}=0, \frac{\partial E}{\partial b_2}=0, \frac{\partial E}{\partial c_2}=0. \qquad (174)
$$

From this we have

$$
\begin{aligned}
&a_2 \int (1 - H(\phi))dxdy + b_2 \int (1 - H(\phi))xdxdy \\
&+c_2 \int y(1 - H(\phi))dxdy = \int u_0(1 - H(\phi)dxdy \\
&a_2 \int x(1 - H(\phi))dxdy + b_2 \int (x^2 + \mu)(1 - H(\phi))dxdy \\
&+c_2 \int xy(1 - H(\phi))dxdy = \int (xu_0 + \mu \frac{\partial u_0}{\partial x})(1 - H(\phi))dxdy \qquad (175) \\
&a_2 \int y(1 - H(\phi))dxdy + b_2 \int xy(1 - H(\phi))dxdy + c_2 \int (y^2 + \mu)(1 - H(\phi))dxdy \\
&= \int (yu_0 + \mu \frac{\partial u_0}{\partial y})(1 - H(\phi))dxdydxdy
\end{aligned}
$$

5.8 Experimental results of the GMS model

We have implemented the GMS model and the MS model using the method developed in [23]. In Figs. 35,36, the segmentation results of an artificial image are shown. It is clear that the piecewise constant and linear approximation MS models can not detect the the correct boundary of the input image. However, the MS model with gradient term and the GMS model can detect the boundary. More importantly, the GMS model can reproduce the texture of the input image.

In Fig. 37, the segmentation results of the piecewise constant MS model, the MS model with gradient term and the GMS model with linear approximation are shown. It is clear that GMS model with linear approximation provides us better results.

5.9 Conclusions

We have applied different variations of the MS model and the ROF model for image segmentation. It is found that the piecewise constant approximation CV model cannot detect the edges with low contrast in the image. For this kind of edges, we need to include the gradient term in the original models. To do this, we can either use the original image to calculate the gradient or use linear approximation of the image function u. Linear approximation ROF-like model is also applied here and we find it produces similar results as the linear approximation of MS model. We also include the Laplacian term in the ROF model and we have found that ROF model with Laplacian

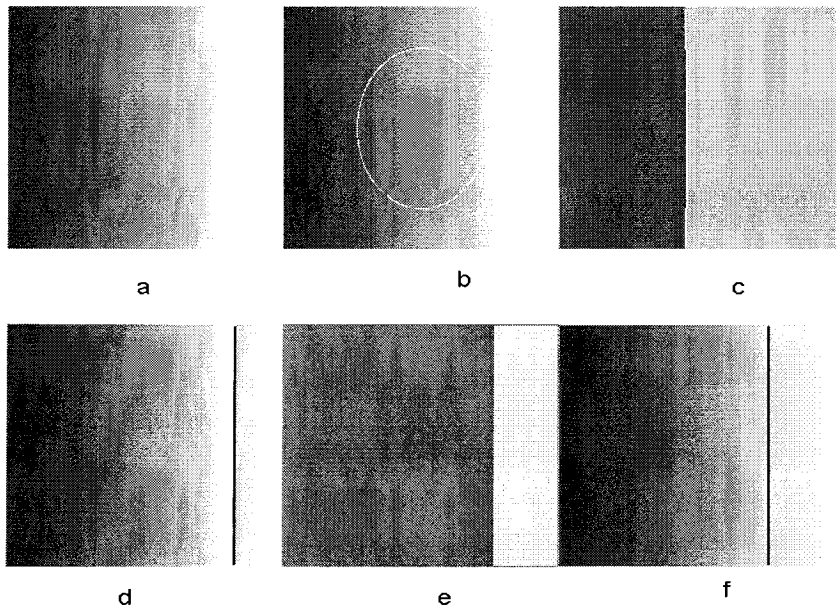

Figure 35: *First row:* (a) : *original image,* (b) : *initial curve.* (c) : *the piecewise constant approximation of the MS model. Second row:* (d) : *MS model with linear approximation,* (e) *The piecewise constant MS model with gradient term,* (f) *GMS model with linear approximation.*

term can produce better results than the piecewise constant approximation CV model.

MS model is generalized to a new model. In this new model, we require that the gradient ∇u approaches ∇u_0. Here u is a approximation to the original image u_0. It is found that with this constraint we can find the roof edge which is hard to be detected by the original MS model.

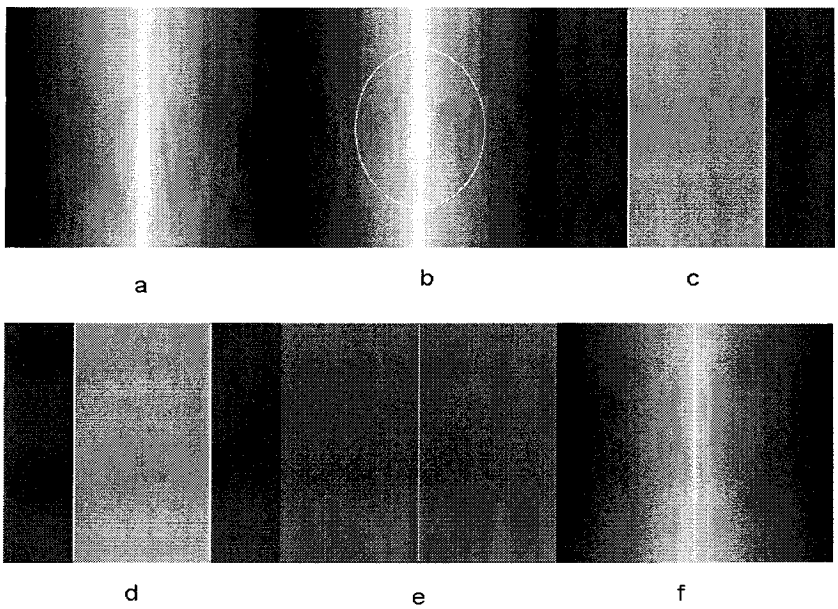

Figure 36: *First row: (a) original image, (b) initial curve. (c) the piecewise constant approximation of the MS model. Second row: (d) MS model with linear approximation, (e) The piecewise constant MS model with gradient term, (f) GMS model with linear approximation.*

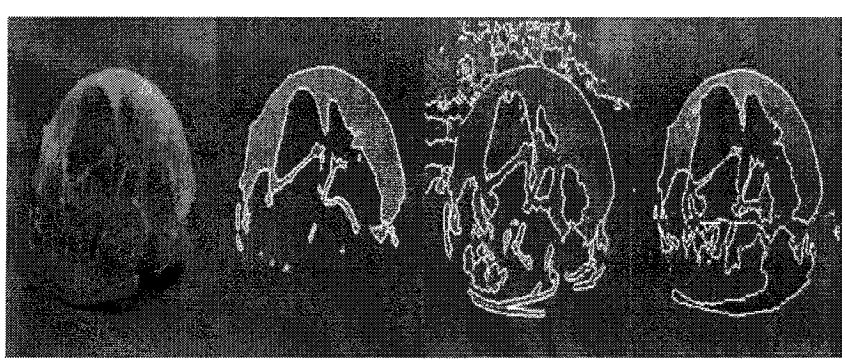

Figure 37: *From left to right: The first image is the originals, the second is the segmentation results of the piecewise constant MS model, the third is the MS model with gradient term, the last is GMS model with linear approximation.*

Chapter 6

Conclusions

In this thesis, we have systematically studied the Mumford-Shah model and its variations and applied to image segmentation problems. The level set method is used in numerical implementation. We have found that the Mumford-Shah model and its variations can produce good segmentation results. It is found that the piecewise constant model can not obtain good segmentation results for images with large intensity variations inside each region. We have proposed a linear approximation to model this kind of images and as expected we have found that this model can produce better segmentation results than the piecewise constant model. We have also proved that the MS energy will decrease with respect to time for both the two-phase and four-phase approaches. A general proof is also given in the Appendix.

The dependence of the Mumford-Shah model on the parameters μ and ν are also investigated. It is found that when $\mu \to \infty$, the piecewise constant MS model results is recovered. On the other hand, if $\mu \to 0$, detailed structure of the images can be obtained. We have also obtained a constraint on the parameter ν for the piecewise constant model.

We have applied different variations of the MS model and the ROF model to images segmentation. In these models we have included the gradient term. To do this, we can either use the original image to calculate the gradient or use linear approximation of the image function u. Linear approximation ROF-like model is also applied here and we find it produces similar results as the linear approximation of MS model. We also include the Laplacian term in the ROF model and we have found that ROF model with Laplacian term can produce better results than the piecewise

constant approximation CV model.

We have generalized the MS model to another model. In this new model, we require that the gradient of the approximation image should approach the gradient of the input image. It is found that with this constraint we can find the roof edge which is hard to be detected by the original MS model.

The segmentation method proposed in this thesis can be extended in several directions. Since the proposed algorithm is based on level set methods, it can be easily extended to solve the image processing problems in higher dimensional space. Therefore, one direction is to extend our segmentation method to three-dimensional image segmentation problems, such as medical image processing. The another direction is to study the μ and ν dependence in the generalized MS model.

Appendix A

A derivation of the Euler-Lagrange equation

A.1 Euler-Lagrange equation for one dependent variable

We will try to minimize $E(u)$

$$inf_u \quad \{E(u) = \int F(x, y, u, u_x, u_y)dxdy\}, \tag{176}$$

with $u = u(x, y), u_x = \frac{\partial u(x,y)}{\partial x}, u_y = \frac{\partial u(x,y)}{\partial y}$. Taking variation of $E(u)$ with u, we have

$$\begin{aligned}
\delta E(u) &= \int [\frac{\partial F}{\partial u}\delta u + \frac{\partial F}{\partial u_x}\delta u_x + \frac{\partial F}{\partial u_y}\delta u_y]dxdy \\
&= \int [\frac{\partial F}{\partial u}\delta u + \frac{\partial F}{\partial u_x}\frac{\partial \delta u}{\partial x} + \frac{\partial F}{\partial u_y}\frac{\partial \delta u}{\partial y}]dxdy \\
&= \int [\frac{\partial F}{\partial u}\delta u + \vec{A} \cdot \nabla(\delta u)]dxdy \\
&= \int [\frac{\partial F}{\partial u}\delta u + \nabla \cdot (\vec{A}\delta u) - \nabla \cdot \vec{A}(\delta u)]dxdy \\
&= \int [\frac{\partial F}{\partial u} - \nabla \cdot \vec{A}]\delta u dxdy + \int (\delta u)\vec{A} \cdot d\vec{l}.
\end{aligned} \tag{177}$$

with

$$\vec{A} = (\frac{\partial F}{\partial u_x}, \frac{\partial F}{\partial u_y}). \tag{178}$$

In the above derivation, we have used Gaussian theorem

$$\int_{\Omega} \nabla \cdot (\vec{A}\delta u)dxdy = \int_{\delta\Omega} (\vec{A}\delta u) \cdot \hat{n}dl. \tag{179}$$

Here $\delta\Omega$ is the boundary of the face Ω and $\hat{n}$ is the normalized normal of the curve $\delta\Omega$.

Since Eq.(177) is true for all δu, we have following equations:

$$\frac{\partial F}{\partial u} - \frac{\partial}{\partial x}(\frac{\partial F}{\partial u_x}) - \frac{\partial}{\partial y}(\frac{\partial F}{\partial u_y}) = 0 \tag{180}$$

and

$$\vec{A} \cdot \hat{n} = \frac{\partial F}{\partial u_x}\frac{\partial x}{\partial \hat{n}} + \frac{\partial F}{\partial u_y}\frac{\partial y}{\partial \hat{n}} = 0. \tag{181}$$

It is clear that this derivation can be generalized to arbitrary number of variables $x_1, x_2, ..., x_n$. Then Eq.(180) changes to

$$\frac{\partial F}{\partial u} - \sum_{i=1}^{n} \frac{\partial}{\partial x_i}(\frac{\partial F}{\partial u_{x_i}}) = 0. \tag{182}$$

We normally refer to Eq.(181) as boundary conditions. In the following, we will denote the left hand side of Eq.(180) as $L(u)$, that is

$$L(u) = \frac{\partial F}{\partial u} - \frac{\partial}{\partial x}(\frac{\partial F}{\partial u_x}) - \frac{\partial}{\partial y}(\frac{\partial F}{\partial u_y}). \tag{183}$$

A.2 Euler-Lagrange equation for more dependent variables

If we have two functions u_1, u_2. Then Eq.(176) changes to

$$inf_u \quad \{E(u_1, u_2) = \int F(x, y, u_1, u_{1x}, u_{1y}, u_2, u_{2x}, u_{2y})dxdy\}, \tag{184}$$

with $u_1 = u_1(x, y), u_2 = u_2(x, y), u_{1x} = \frac{\partial u_1(x,y)}{\partial x}, u_{1y} = \frac{\partial u_1(x,y)}{\partial y}, u_{2x} = \frac{\partial u_2(x,y)}{\partial x}, u_{2y} = \frac{\partial u_2(x,y)}{\partial y}$. Taking variation of $E(u_1, u_2)$ with u_1, we have (similar to Eq.(177))

$$\delta E(u_1) = \int [\frac{\partial F}{\partial u_1}\delta u + \frac{\partial F}{\partial u_{1x}}\delta u_x + \frac{\partial F}{\partial u_{1y}}\delta u_y]dxdy$$

$$= \int [\frac{\partial F}{\partial u} - \nabla \cdot \vec{A_1}] \delta u_1 dxdy + \int (\delta u_1) \vec{A_1} \cdot d\vec{l}. \tag{185}$$

with

$$\vec{A_1} = (\frac{\partial F}{\partial u_{1x}}, \frac{\partial F}{\partial u_{1y}}). \tag{186}$$

In the above derivation, we have used Gaussian theorem

$$\int_\Omega \nabla (\vec{A_1} \delta u_1) dxdy = \int_{\delta\Omega} (\vec{A_1} \delta u_1) \cdot \hat{n} dl. \tag{187}$$

Here $\delta\Omega$ is the boundary of the face Ω and $\hat{n}$ is the normalized normal of the curve $\delta\Omega$.

Since Eq.(185) is true for all δu_1, we have following equations:

$$\frac{\partial F}{\partial u_1} - \frac{\partial}{\partial x}(\frac{\partial F}{\partial u_{1x}}) - \frac{\partial}{\partial y}(\frac{\partial F}{\partial u_{1y}}) = 0 \tag{188}$$

and

$$\vec{A_1} \cdot \hat{n} = \frac{\partial F}{\partial u_{1x}} \frac{\partial x}{\partial \hat{n}} + \frac{\partial F}{\partial u_{1y}} \frac{\partial y}{\partial \hat{n}} = 0. \tag{189}$$

We can derive a similar formula for u_2. That is

$$\frac{\partial F}{\partial u_1} - \frac{\partial}{\partial x}(\frac{\partial F}{\partial u_{2x}}) - \frac{\partial}{\partial y}(\frac{\partial F}{\partial u_{2y}}) = 0 \tag{190}$$

and

$$\vec{A_2} \cdot \hat{n} = \frac{\partial F}{\partial u_{2x}} \frac{\partial x}{\partial \hat{n}} + \frac{\partial F}{\partial u_{2y}} \frac{\partial y}{\partial \hat{n}} = 0. \tag{191}$$

with

$$\vec{A_2} = (\frac{\partial F}{\partial u_{2x}}, \frac{\partial F}{\partial u_{2y}}). \tag{192}$$

This derivation can be generalized to more functions (we will denote them as $u(1), u(2), ..., u(m)$),then Eq.(176) becomes

$$\begin{aligned} &inf_{u(1),u(2),..,u(m)} \quad \{E(u(1), u(2), ..., u(m)) = \int F(x_1, x_2, ..., x_n, \\ &u(1), u(1)_{x_1}, u(1)_{x_2}, ..., u(1)_{x_n}, u(2), u(2)_{x_1}, u(2)_{x_2}, ..., u(2)_{x_n}, ..., \\ &u(m), u(m)_{x_1}, u(m)_{x_2}, ..., u(m)_{x_n},) dx_1 dx_2 ... dx_n\}, \end{aligned} \tag{193}$$

with $u(j) = u(j)(x_1, x_2, ..., x_n), u(j)_{x_i} = \frac{\partial u(j)(x_1,x_2,...,x_n)}{\partial x_i}$. Then we will have Euler-Lagrange equations

$$\frac{\partial F}{\partial u(j)} - \sum_{i=1}^{n} \frac{\partial}{\partial x_i}(\frac{\partial F}{\partial u(j)_{x_i}}) = 0 \qquad (j = 1, ..., m). \tag{194}$$

Appendix B

Proof of $\frac{\partial E}{\partial t} \leq 0$

B.1 One dependent variable case

To solve Eq.(180) with boundary conditions of Eq.(181) in Appendix A, we normally use the gradient technique. That is, we change Eq.(180) to the following time dependent equation

$$\frac{\partial u}{\partial t} = G(u). \tag{195}$$

If this equation has a stable solution as time goes to infinity, that is $\frac{\partial u}{\partial t}|_{t\to\infty} = 0$, then we have $G(u) = 0$. If as long as G(u)=0, $L(u) = 0$, then the solution of Eq.(195) is also a solution of Eq.(180).

In the following, we will show that we can choose a function of $G(u)$ such that its solution will minimize the energy $E(u)$ in Eq.(176).

From Eq(195), u is a function of time; accordingly, $E(u)$ is also a function of time. Thus we have

$$\begin{aligned}
\frac{\partial E}{\partial t} &= \int [\frac{\partial F}{\partial u}\frac{\partial u}{\partial t} + \frac{\partial F}{\partial u_x}\frac{\partial u_x}{\partial t} + \frac{\partial F}{\partial u_y}\frac{\partial u_y}{\partial t}]dxdy \\
&= \int [\frac{\partial F}{\partial u}u_t + \frac{\partial F}{\partial u_x}\frac{\partial u_t}{\partial x} + \frac{\partial F}{\partial u_y}\frac{\partial u_t}{\partial y}]dxdy \\
&= \int [\frac{\partial F}{\partial u}u_t + \vec{A}\cdot\nabla(u_t)]dxdy \\
&= \int [\frac{\partial F}{\partial u}u_t + \nabla\cdot(\vec{A}u_t) - \nabla\cdot\vec{A}(u_t)]dxdy \\
&= \int [\frac{\partial F}{\partial u} - \nabla\cdot\vec{A}]u_t dxdy + \int (u_t)\vec{A}\cdot d\vec{l}.
\end{aligned} \tag{196}$$

with

$$\vec{A} = (\frac{\partial F}{\partial u_x}, \frac{\partial F}{\partial u_y}), u_t = \frac{\partial u}{\partial t}. \tag{197}$$

In the above derivation, we have used Gaussian theorem (Eq.(179)). Using the definition of $L(u)$ (Eq.(183)), we have

$$\frac{\partial E}{\partial t} = \int L(u)u_t + \int (u_t)\vec{A} \cdot d\vec{l}. \tag{198}$$

The last term of Eq.(198) is zero due to the boundary conditions in Eq.(181). Using Eq.(195), we have

$$\frac{\partial E}{\partial t} = \int L(u)G(u). \tag{199}$$

It is clear that if we take $G(u) = -L(u)$, then

$$\frac{\partial E}{\partial t} \leq 0. \tag{200}$$

Therefore, the solution of Eq.(195) is the solution of the Eq.(176) which will minimize the energy functional $E(u)$ in Eq.(176).

We have also noticed that if we take $E(L(u)) = L(u)$, then we will have

$$\frac{\partial E}{\partial t} \geq 0. \tag{201}$$

Then the corresponding solution of Eq.(195) will give us a maximum value of E. Therefore the choice of $E(L(u))$ is very important when we change the Euler-Lagrange equation to the time dependent equation.

B.2 Two dependent variables

Using gradient projection method, we have the following equations

$$\frac{\partial u_1}{\partial t} = G_1(u), \quad \frac{\partial u_2}{\partial t} = G_2(u). \tag{202}$$

Similar to Eq.(196), we have

$$\frac{\partial E(u_1, u_2)}{\partial t} = \int [\frac{\partial F}{\partial u_1}\frac{\partial u_1}{\partial t} + \frac{\partial F}{\partial u_{1x}}\frac{\partial u_{1x}}{\partial t} + \frac{\partial F}{\partial u_{1y}}\frac{\partial u_{1y}}{\partial t}]dxdy$$

$$
\begin{aligned}
&+\int[\frac{\partial F}{\partial u_2}\frac{\partial u_2}{\partial t}+\frac{\partial F}{\partial u_{2x}}\frac{\partial u_{2x}}{\partial t}+\frac{\partial F}{\partial u_{2y}}\frac{\partial u_{2y}}{\partial t}]dxdy \\
= &\int[\frac{\partial F}{\partial u_1}u_{1t}+\frac{\partial F}{\partial u_{1x}}\frac{\partial u_{1t}}{\partial x}+\frac{\partial F}{\partial u_{1y}}\frac{\partial u_{1t}}{\partial y}]dxdy \\
&[\frac{\partial F}{\partial u_2}u_{2t}+\frac{\partial F}{\partial u_{2x}}\frac{\partial u_{2t}}{\partial x}+\frac{\partial F}{\partial u_{2y}}\frac{\partial u_{2t}}{\partial y}]dxdy \\
= &\int[\frac{\partial F}{\partial u_1}u_{1t}+\vec{A_1}\cdot\nabla(u_{1t})]dxdy \\
&+\int[\frac{\partial F}{\partial u_2}u_{2t}+\vec{A_2}\cdot\nabla(u_{2t})]dxdy \\
= &\int[\frac{\partial F}{\partial u_1}u_{1t}+\nabla\cdot(\vec{A_1}u_{1t})-\nabla\cdot\vec{A_1}(u_{1t})]dxdy \\
&+\int[\frac{\partial F}{\partial u_2}u_{1t}+\nabla\cdot(\vec{A_2}u_{2t})-\nabla\cdot\vec{A_2}(u_{2t})]dxdy \\
= &\int[\frac{\partial F}{\partial u_1}-\nabla\cdot\vec{A_1}]u_{1t}dxdy+\int(u_{1t})\vec{A_1}\cdot d\vec{l}. \\
&+\int[\frac{\partial F}{\partial u_2}-\nabla\cdot\vec{A_2}]u_{2t}dxdy+\int(u_{2t})\vec{A_2}\cdot d\vec{l}. \qquad (203)
\end{aligned}
$$

with

$$
\vec{A_1}=(\frac{\partial F}{\partial u_{1x}},\frac{\partial F}{\partial u_{1y}}),u_{1t}=\frac{\partial u_1}{\partial t},\vec{A_2}=(\frac{\partial F}{\partial u_{2x}},\frac{\partial F}{\partial u_{2y}}),u_{2t}=\frac{\partial u_2}{\partial t}. \qquad (204)
$$

In the above derivation, we have used Gaussian theorem (Eq.(179)). Using the definition of $L_1(u)$ and $L_2(u)$ which are LHSs of Eq.(188) and Eq.(190), we have

$$
\frac{\partial E}{\partial t}=\int(L_1(u)u_{1t}+L_2(u)u_{2t})dxdy+\int(u_{1t})\vec{A_1}\cdot d\vec{l}.+\int(u_{2t})\vec{A_2}\cdot d\vec{l}. \qquad (205)
$$

The last two terms of Eq.(205) is zero due to the boundary conditions in Eq.(189) and Eq.(191). Using Eq.(202), we have

$$
\frac{\partial E}{\partial t}=\int[L_1(u)G_1(u)+L_2(u)G_2(u)]dxdy. \qquad (206)
$$

It is clear that if we take $G_1(u)=-L_1(u)$ and $G_2(u)=-L_2$, then

$$
\frac{\partial E}{\partial t}=-\int(L_1^2+L_2^2)dxdy\leq 0. \qquad (207)
$$

Therefore, the solution of Eq.(202) is the solution of the Eq.(184) which will minimize the energy functional $E(u)$ in Eq.(184).

Bibliography

[1] G. Aubert and P. Kornprobst, Mathematical Problems in Image Processing: Partial differential equations and the Calculus of Variations, Vol. 147 of Applied Mathematical Sciences, Springer-Verlag, 2002.

[2] V. Caselles, R. Kimmel, and G. Sapiro, Geodesic active contours, The International Journal of Computer Vision, 1997, 22(1): 61-79.

[3] V. Caselles, R. Kimmel, and G. Sapiro,Geodesic active contours, In Proceedings of the 5-th International Conference on Computer Vision, pp. 694-699, MA, June 1995, IEEE Computer Society Press.

[4] S. Kichenassamy, A. Kumar, P. Olver, A. Tannenbaum, and A. Yezzi, Conformal curvature flows: from phase transition to active vision. Archive for Rational Mechanics and analysis, 134: 275-301, 1996.

[5] S. Kichenassamy, A. Kumar, P. Olver, A. Tannenbaum, and A. Yezzi, Gradient flows and Geometric active contour models, in Proceedings of the 5th international Conference on computer Vision, pp.810-815, Boston, MA, June 1995, IEEE Computer Society Press.

[6] T. F. Chan and L. A. Vese, Active Contours without edges, IEEE transactions on Image Processing, 2001, 10(2): 266-277.

[7] P. Charbonnier, L. Blanc-Feraud, G. Aubert, and M. Barlaud, Deterministic edge-preserving regularization in computer imaging, IEEE Trans. Image Process. 6, 1997, 298-311.

[8] S. Gao and Tien D. Bui, Image segmentation and selective smoothing by using Mumford-Shah model, to be published in IEEE Trans. on Image Processing.

[9] S. Gao and Tien D. Bui, A new image segmentation and smoothing model, Proc. of IEEE int. Symposium on Biomedical Imaging: From Nano to Macro, pp. 137-140, Arlington, V.A., April 15-18, 2004.

[10] M. Kass, A. Witkin, and D. Terzopoulos, snake, Active Contour Models, The International Journal of Computer Vision 1, pp321-331, 1988.

[11] B. R. Lee, A. Ben Hamza and H. Krim, An active contour model for image segmentation: a variational perspective. Proc. IEEE international conference on acoustics speech and Signal processing, Orlando, May 2002.

[12] S. Z. Li, Roof-Edge Preserving Image Smoothing Based on MRFs, IEEE Transactions On Image Processing, Vol. 9, No. 6, June 2000, pp.1134-1138.

[13] D. Mumford, and J. Shah, Optimal approximation by piecewise smooth functions and associated variational problems. Comm. Pure Appl. Math. 42 (1989) 577 - 685.

[14] S. Osher and J. Sethian, Fronts propagating with curvature-dependent speed : Algorithm based on the Hamilton-Jacobi formulation, Journal of Computational physics, 79 pp12-49, 1988.

[15] F.A. Pellegrino, W. Vanzella, and V. Torre, Edge Detection Revisited, IEEE Transactions On Systems, Man, And Cybernetics Part B: Cybernetics, Vol. 34, No. 3, June 2004, pp.1500-1517.

[16] J. A. Sethian, level Set Methods and Fast Marching Methods, Cambridge University Press, 1999.

[17] B. Song and T. F. Chan, A Fast Algorithm for Level Set Based Optimization, UCLA CAM Report 02-68 (December 2002).

[18] S. Teboul, L. Blanc-Feraud, G. Aubert, and M. Barlaud, Variational Approach for Edge-Preserving Regularization Using Coupled PDEs, IEEE Transactions On Image Processing, Vol. 7, No. 3, March 1998 387-397.

[19] A. Tsai, A. Yezzi, and Alan S. Willsky, Curve Evolution Implementation of the Mumford-Shah Functional for Image Segmentation, Denoising, Interpolation,

and Magnification, IEEE Tran. on Image Processing, Vol. 10 (8), 2001, 1169-1186.

[20] A. Yezzi, A. Tsai, and A. Willsky, " A statistical approach to snakes for bimodal and trimodal imagery," in Proc. Int. Conf. Computer Vision, 1999.

[21] L. Vese and T. F. Chan, A multiphase Level Set Framework for Image Segmentation Using the Mumford and Shah Model, International Journal of Computer Vision 50(3), 271-293, 2002.

[22] T. Chan, J. Shen, and L. Vese, "Variational PDE Models in Image Processing," Notices of the American Mathematical Society, vol. 50, no. 1, pp. 14-26, Jan.,2003.

[23] T. Chan and L. Vese, " A level set algorithm for minimizing the Mumford-Shah functional in Image Processing," IEEE/Computer Society Proceedings of the 1st IEEE Workshop on "Variational and Level Set Methods in Computer Vision", pp. 161-168, 2001.

[24] T. F. Chan, B. Y. Sandberg, and L. A. Vese, "Active Contours without Edges for Vector-Valued Images", Journal of Visual Communication and Image Representation vol 11, pp.130-141, 2000.

[25] L. A. Vese, Multiphase Object Detection and Image Segmentation, in "Geometric Level Set Methods in Imaging, Vision and Graphics", S. Osher and N. Paragios (eds), Springer Verlag, 2003, pp. 175-194.

[26] J. Weickert, Anisotropic diffusion in Image Processing, Teubner, Stuttgart (1998).

[27] R.A. Weisenseel, W.C. Karl, D.A. Castanon, A region-based alternative for edge-preserving smoothing, Proceedings of the International Conference on Image Processing, 2000. pp. 778-781. Vancouver, BC, Canada.

[28] S.Z. Li, Markov Random Field Modeling in Image Analysis, Springer, 2001.

[29] S. Geman, and D. Geman, Stochastic Relaxation, Gibbs Distribution, and the Bayesian Restoration of Images. IEEE Trans. on PAMI. 6 (1984) 721-741.

[30] A. Blake and A. Zisserman, Visual Reconstruction, The MIT Press Cambridge, Massachusetts, 1987.

[31] S. Osher and N. Paragios, Geometric Level Set Methods, Springer, 2003.

[32] S. Osher and R. P. Fedkiw, " Level set Methods: An overview and some recent results," Journal of Computational Physics, vol. 169, pp.463-502, 2001.

[33] D. Adalsteinsson, and J. A. Sethian, " A Fast Level set methods for Propagating Interfaces," Journal of Computational Physics, vol. 118, no. 2, pp.269-277, 1995.

[34] H. K. Zhao, T. F. Chan, B. Merriman, S. Osher, " A Variational Level Set Approach to Multiphase Motion", Journal of Computational Physics, vol. 127, pp. 179-195, 1996.

[35] S. Osher and R. P. Fedkiw, Level set Methods and Dynamic Implicit Surfaces, Springer Verlag, 2002.

[36] L. Rudin, S. Osher and E. Fatemi, Nonlinear total variation based noise removal, Physica D, Vol. 60 , 1992, 259-268.

[37] W. Vanzella, F.A. Pellegrino, and V. Torre, Self-Adaptive Regularization, IEEE Transactions On PAMI, Vol. 26, No. 6, June 2004, pp.804-809.

[38] S. Geman and D. Geman, "Stochastic relaxation, Gibbs distributions, and the Bayesian restoration of images", IEEE Trans. Patt. Anal. and Mach. Intell., vol. 6, no 6, pp721-741, November 1984.

[39] E. Y. Kim, S. H. Park, and H. J. Kim, "A Genetic Algorithm-Based-Segmentation of Markov Random Field Modeled Images," IEEE Signal Processing Letters, vol 7, no 11, pp.301-303, 2000.

[40] A. Sarkar, M. K. Biswas, and K. M. S. Shama, " A simple Unsupervised MRF Model Based Image Segementation Approach," IEEE Transactions on Image Processing, vol. 0, no. 5, pp.801-812,2000.

[41] R. Wilson and M. Spann, Image segmentation and Uncertainty, John Wiley & Sons Inc. 1988.

[42] J. C. Russ, the Image Processing Handbook, CRC press, Inc, 1992.

[43] T. D. Bui, S. Gao and Q. H. Zhang, A generalized Mumford-Shah model for roof edges detection, to be published in the proceeding of ICIP, Sept. 11-14, 2005, Genova, Italy.

[44] Q. H. Zhang, S. Gao and T. D. Bui, A roof edge detection model, to be published the proceeding of IbPRIA, June 7-9, 2005, Estoril, Portugal.

[45] Q. H. Zhang, S. Gao and T. D. Bui, Edge detection models, to be published in the proceeding of ICIAR, Sept. 28-30, 2005, Toronto, Canada.

[46] S. Gao, "A New Image Segmentation and Smoothing Method Based on the Mumford-Shah Variational Model", Master thesis in Computer Science Department, Concordia University, 2003.

[47] H. K. Zhao, S. Osher, B. Merriman, and M. Kang, "Implicit and Nonparametric Shape Recognition from Unorganized Data Using a Variational Level set Method", Computer Vision and Image understanding, vol. 80, pp. 295-314, 2000.

[48] I. Sobel, " An isotropic 3X3 image gradient operator, " In Machine Vision for Three Dimensional Scenes, edited by H. Freeman, Academic Press, pp. 376-379, 1990.

[49] J. Canny, " A Computational approach for edge detection, "IEEE Transaction on Patttern Anal. Machine Intell. , vol 8, no 6, pp679-698,1986.

[50] R. Deriche, "Using Canny's criteria to derive a recursive implemented optimal edge detector, " The international Journal of Computer Vision, vol. 1, no 2, pp.167-187, 1987.